GPS Observations of Ionospheric TEC Variations during 2015 Mw 7.8 Nepal Earthquake

M. Karki[1], A. Silwal[2], N. P. Chapagain[1], P. Poudel[2], S. P. Gautam[3], R. K. Mishra[4], B. Adhikari[4, *]
Yenca Migoya-Orue[5]

[1] Amrit Campus, Tribhuvan University, Kathmandu, Nepal

[2] Patan Multiple Campus, Tribhuvan University, Lalitpur, Nepal

[3]Central Department of Physics, Tribhuvan University, Kirtipur, Nepal

[4]Department of Physics, St. Xavier College, Maitighar, Kathmandu

[5]T/ICT4D laboratory of the Abdus Salam International Center for Theoretical Physics, 34151 Trieste, Italy

*__Corresponding author__: binod.adhi@gmail.com

Abstract

Ionospheric total electron content (TEC) variations prior and after to the great Gorkha Earthquake in Nepal (Mw = 7.8) on April 25, 2015, were analysed using measurements from widely distributed Global Positioning System (GPS) network. This study has been performed to understand the relationship between ionospheric TEC anomalies and earthquake occurrences. The analysis of vertical TEC (VTEC) time series from different GPS stations shows that the abnormal TEC variations appeared few days up to a few hours before the events. The results indicate that deviation in VTEC observed on the distant GPS station from the epicentre was found less relative to that of the stations near the epicentre, inferring that the variation in ionospheric VTEC nearly inversely relies upon the distance of GPS stations from the epicentre. Moreover, the pre-earthquake ionospheric anomalies were also observed in the geomagnetically conjugated region. In view of the solar-terrestrial environment, the pre-earthquake ionospheric anomalies could be associated with the Nepal earthquake. The VTEC anomaly was identified when it crosses the upper bound or lower bound. The outcomes additionally show that TEC variation was dominant in the vicinity of the earthquake epicentre. We also describe contrast in TEC throughout the globe using global ionospheric maps at regular 2-hour UT intervals, the day before, during and after the earthquake. In addition, we observed that areas heavily influenced by TEC were found to be transposed from eastern sectors to western sectors through the equatorial plane. TEC Maps indicate that most of the Indian areas, Northern China, Nepal, Bhutan, were heavily affected, addressing the earthquake's onset effect. During the day of the occurrence and one of the quietest days, we also tested the cross-correlation of TEC of SGOC from Srilanka station and various other stations; the correlation steadily increased by epicentral distance with the surrounding stations, which was another fascinating result. Thus, these findings showed that the influence of the earthquake was seen

globally, with the conclusion that the variation of TEC over various stations of the globe could turn out to be very helpful in predicting the earthquake.

Keywords: Earthquake, Ionosphere, Total Electron Content, Seismic Waves

Introduction

The ionosphere is a complex layer in the upper part of the atmosphere which undergoes both spatial and temporal change mainly because of the ionization effect of high-energetic solar radiation of extreme ultraviolet (EUV) and solar-related ionospheric disturbances (Rana et al., 2019). The Earth sends transient signals, sometimes stronger and more often subtle and more transitory, according to ionospheric studies, before major earthquakes which often showed the temporary disturbances within the ionosphere (Pulinets, 2007; Sharma et al., 2017). All energy input into the ionosphere was predominantly clarified by the sources from solar and geomagnetic influences, while other influences on the ionosphere were essentially ignored (Pulinets et al., 1998). A significant number of worldwide research groups are studying ionospheric perturbations prior to big earthquakes (Liu et al., 2000; Pulinets, 2002; Pulinets et al., 2005; Sharma et al., 2017; Shi et al., 2020). Earthquakes are one of nature's most destructive and unforeseen natural phenomenon. The unexpected fault rupture results into the sudden release of energy that stored in Earth's crust creating seismic waves (Ohnaka, 2013). Over the history of earthquakes, many people have been killed and many localities of the country have been devastated. Numerous attempts have also been made to use parameters to predict earthquakes using a variety of phenomena, such as Ionosonde, seismicity pattern (Wang et al. 2010), radon or hydrogen gas (Planini et al., 2004) and space-based observations of energetic electron precipitation (Kudela et al., 1992). Different techniques can be used to detect the ionospheric perturbations namely Global Positioning System (GPS)-Total electron content (TEC) measurements (Pulinets, 2002; Haase, 2011), COSMOS Satellite measurements, DEMETER Satellite measurements (Pisa et al., 2012) etc. TEC is the total number of electrons present along a path between two points, with units of electrons per square meter, where 10^{16} electrons/m^2 =1 TEC unit (TECU) (Klobuchar, 1991, Adhikari et al., 2019). Based on these observations, ionospheric electron contents have been established as one of the key ionosphere parameters and can be applied to detect a pre-earthquake ionospheric anomaly. GPS / GNSS stations are being deployed globally and have become an important tool to research ionospheric TEC before major earthquakes. Jiang (2017) investigated the ionospheric VTEC before 2014, Mw 8.2 Chile earthquake and observed positive anomalies 4 days before the main earthquake.

The connection between ionospheric TEC anomalies and earthquake occurrences is ultimately governed by the lithosphere-atmosphere-ionosphere coupling mechanism (Pulinets, 2004). The ionosphere records the earthquake-induced by the change in the global electrical circuit triggered by

the accumulation of ions in the atmosphere, originating due to the development of stress in the crustal region prior to an earthquake (Pulinets, 2004; Friedemann and Kulahci, 2009; Sharma et al., 2017). Pullinets (2004) gave a detailed description of the process of ion cluster formation in the near-ground layer in the earthquake preparation zone. Ionospheric TEC has many difficulties for earthquake precursor studies to resolve, primarily due to lack of adequate observation stations and complications in the results of TEC data resulting from different factors. (Pullinets, 2007, 2009). Several studies reported the GPS derived TEC anomalies from 0 to 8 days before major seismic events (Pulinets, 2009; Liu et al., 2011; Sharma et al., 2017).

Nepal is a seismically active region of the world where there has been a devastating earthquake in the past. On April 25 2015, a large magnitude (Mw 7.8) earthquake occurred at 11:56 Nepal Standard Time (NST) (06:11:25 UTC) with an epicentre at 28.1473 ^{0}N and 84.708 ^{0}E, 8.2 km depth, 34 km east-southeast of Lamjung, Nepal (Adhikari et al., 2020). The main-shock was followed by two large aftershocks of Mw 6.7 (on 26 April 2015 at 09:10 UTC) and Mw 7.3 (on 12 May at 07:05 UTC).

In this present work, we report the disturbances of the ionosphere TEC observed by GPS TEC measurements from locations near and far from the epicentre during the April 2015 Nepal earthquake. Some new findings are drawn by studying the ionospheric TEC deviation and cross-correlation between the various GPS stations. In addition, we have used the Global Ionospheric Map (GIM) to detect TEC variation across the globe. Continuous monitoring of GIM provides an alternative way of measuring the global effects of natural disasters such as earthquakes on the ionosphere and could be used as a sophisticated tool to forecast the emergence of these natural events.

2. Data and Method

In this study, data from nine UNAVCO GPS stations have been used to recognize coseismal TEC perturbations caused by 2015 Nepal earthquake. Table 1 provides comprehensive information on the nine selected GPS stations with their geographic latitude and longitude. We analysed GPS data of 30s sampling interval from two (HYDE, IISC) Indian sites, from one (SGOC) Srilanka site and 15s sampling interval from six sites (CHLM, NPGJ, KKNI, DNSG, JMSM, DNDG) of Nepal. The calibrated VTEC, captured with a time resolution of 15 sec and 30 sec was later converted to 1hr resolution by taking the average with the proper selection of time interval (1hr = 3600s). The vertical TEC data were taken from the dual-frequency carrier phases and differential code recorded by ground-based GPS receivers during the interval of 1 month, including both prior to the earthquake. The raw data from GPS station were pre-processed to convert into the receiver exchange format (RINEX). A RINEX file from the selected GPS stations was processed in order to

calculate vertical TEC by the help of the calibration algorithm (Ciraolo, 1993). It assumes that ionosphere is concentrated within a thin shell located at around 357-457 km of altitude (Oikonomou et al., 2016). The slant range TEC (STEC) can be obtained from a satellite to a receiver as the dual-frequency carrier-phase observations L_1 and L_2 (Chen et al., 2016; Shi and Guo et al., 2019) as per the following equation:

$$STEC = \frac{(f1f2)^2}{40.3(f1^2 - f2^2)} (L_1 - L_2 + \lambda_1 (N_1 + b_1) - \lambda_1 (N_2 + b_2) + \varepsilon_L \quad \ldots\ldots\ldots\ldots (1)$$

where f1 and f2 are GPS signal frequencies at 1575.42 MHz and 1227.60 MHz; λ is the signal wavelength; N is ambiguity; b is the instrument biases for carrier phase; ε is residuals. The vertical TEC can be obtained by converting STEC as:

$$VTEC = STEC \times \cos\left(\arcsin\left(\frac{R.sin\alpha}{R+H}\right)\right) \quad \ldots\ldots\ldots\ldots (2)$$

where R is the Earth radius; α is the elevation angle of the satellite; H is the height of the ionosphere. We have chosen height at an altitude of 400 km for our analysis. For the identification of seismo-ionospheric signal, we have observed the behaviour of VTEC for 30 running days by statistical analysis (Liu et al., 2004; Sharma et al., 2017). To construct the upper and lower bounds, we have computed the median (μ) and standard deviation (σ) of 15 running days written as:

$$\text{Upper Bound (UB)} = \mu + 1.34\,\sigma \quad \ldots\ldots\ldots\ldots (3)$$

$$\text{Lower Bound (LB)} = \mu - 1.34\,\sigma \quad \ldots\ldots\ldots\ldots (4)$$

If the VTEC value crosses the UB and LB, then the positive (high) and negative (low) anomalies are considered respectively (Liu et al., 2009; Yao and Chen et al., 2012), an abnormal signal was detected at a confidence level of about 82% (Kotz and Johnson, 1982; Oikonomou et al., 2016). In addition to our analysis, for the same period of days, we also plotted the geomagnetic indices; Dst (nT) and Ap (nT) along with the f10.7 solar index in order to ensure that there were no inputs from geomagnetic activities on the event period and the detected ionospheric perturbations can be guaranteed as a consequence of the earthquake.

Table 1: Detailed information on GPS stations with their geographical latitude and longitude and distance from the epicentre.

GPS Station	**Geographical Latitude (^{0}N)**	**Geographical Longitude (^{0}E)**	**Distance from the epicentre (km)**
CHLM	28.2072	85.3141	57.1

NPGJ	28.1172	81.5953	307.61
KKNI	27.8007	85.2788	71.9
JMSM	28.8053	83.7433	115.8
DNGD	28.7544	80.5818	409.7
DNSG	28.3451	83.7635	95.6
HYDE	17.4173	78.5579	1358.64
SGOC	6.8921	79.8742	2427.802
IISC	13.0212	77.5704	1148.146

Cross-Correlation

Cross-correlation is the standard statistical technique to study the relationship among different variables along with timely analysis and draw the identical characters to probe the new information (Usoro, 2015; Adhikari et al., 2017). In this present study, the cross-correlation technique has been employed to establish the similarity pattern of different GPS stations in order to verify the abrupt variation in VTEC value on 25th April 2015. The correlation coefficient is scaled from -1 to +1 and the curve indicates strong correlation when it is close by ±1, whereas correlation coefficient around zero displays moderate or less correlation between the variables (Katz, 1988; Adhikari et al., 2018).

Results and Discussion

In this section, we addressed the ionospheric response to April 25, 2015, Nepal earthquake (M_w 7.8) from GPS measurements recorded over a network of receivers which are distributed in the epicentral region of the earthquake and sites quite far from the epicentre.

Time Series Analysis for the month of April 2015

In this study, we have attempted to investigate the time-series of TEC anomalies which are expected for April 25 2015, Nepal earthquake**.** The TEC time-evolution analysis was carried out using six GPS observations stations located at 57-500 km areal distance from the epicentre of the earthquake. Time- series analysis of TEC for a period of 30 days was carried out to observe the diurnal TEC variations, along with corresponding upper and lower bounds of TEC values. Fig 1 shows the 30 days TEC time-series observations with associated upper and lower bounds prior to and after to

earthquake. TEC variations preceding Nepal earthquake started almost a few days before the event. A prominent positive (high) anomaly crossing upper boundary layer was observed on 2nd, 3rd, 14th, 16th, 17th and 24th prior to mainshock (25th April 2015) and low TEC value was observed on 11th April prior to and on 29th April 2015 after to mainshock at CHLM GPS station located at 57.1 km distance from the epicentre. The low TEC value observed was attributed to the reversal of electric field direction as postulated by Pulinets, (1998) and Sharma et al., (2017). In order to check the consistency of TEC anomalies, similar anomalies were expected to be observed from other stations. The analysis shows similar patterns in TEC anomalies from all six observations stations. Additionally, at other observatories GPS station, the analysis revealed high TEC anomalies crossing UBL on the same anomaly days that we observed at CHLM station except for 29th April, with including 4th April 2015 prior to the main event at DNGD located at a distance of 409.7 km from the epicentre. Observations at KKNI and NPGJ GPS stations located at a distance of 71.9 km and 307.61 km respectively indicate high TEC anomaly on 5th and 23rd April before the earthquake. TEC derived from DNSG and JMSM located at a distance of 95.6 km and 115.8 km respectively showed similar anomalies like other stations. In addition to the mainshock on April 25, 2015, it was followed by big aftershocks on the same day as well as on 26th April with a magnitude of 6.7 at around 12:54:08 NST (07:08 UTC), with an epicentre located about 17 km south of Kodari, Nepal (USGS earthquake catalogue). These anomalies were also checked with other geomagnetic indices (Dst, Ap and f10.7) to detect the effect of a geomagnetic storm as shown in fig 2. It was observed that these anomalies were not affected by any geomagnetic phenomenon except for 16th and 17th of April. The change in TEC depends on solar activity, geomagnetic storm and receiving GPS station location and also varies with time and space. The energy and currents released by a geomagnetic storm increase the total height-integrated number of ionospheric TEC (Sharma et. al., 2017). Increase in ionospheric TEC results in the spatial variability of the ionosphere and cause ionospheric delays in the GPS signals (Pulinets, 2009). Overall, the TEC values corresponding to the anomaly time from all six stations was observed that the earthquakes had at least one high TEC value crossing UBL and low TEC value crossing LBL which was also observed in earlier studies (Sharma et al., 2017, 2018, 2019, 2020).

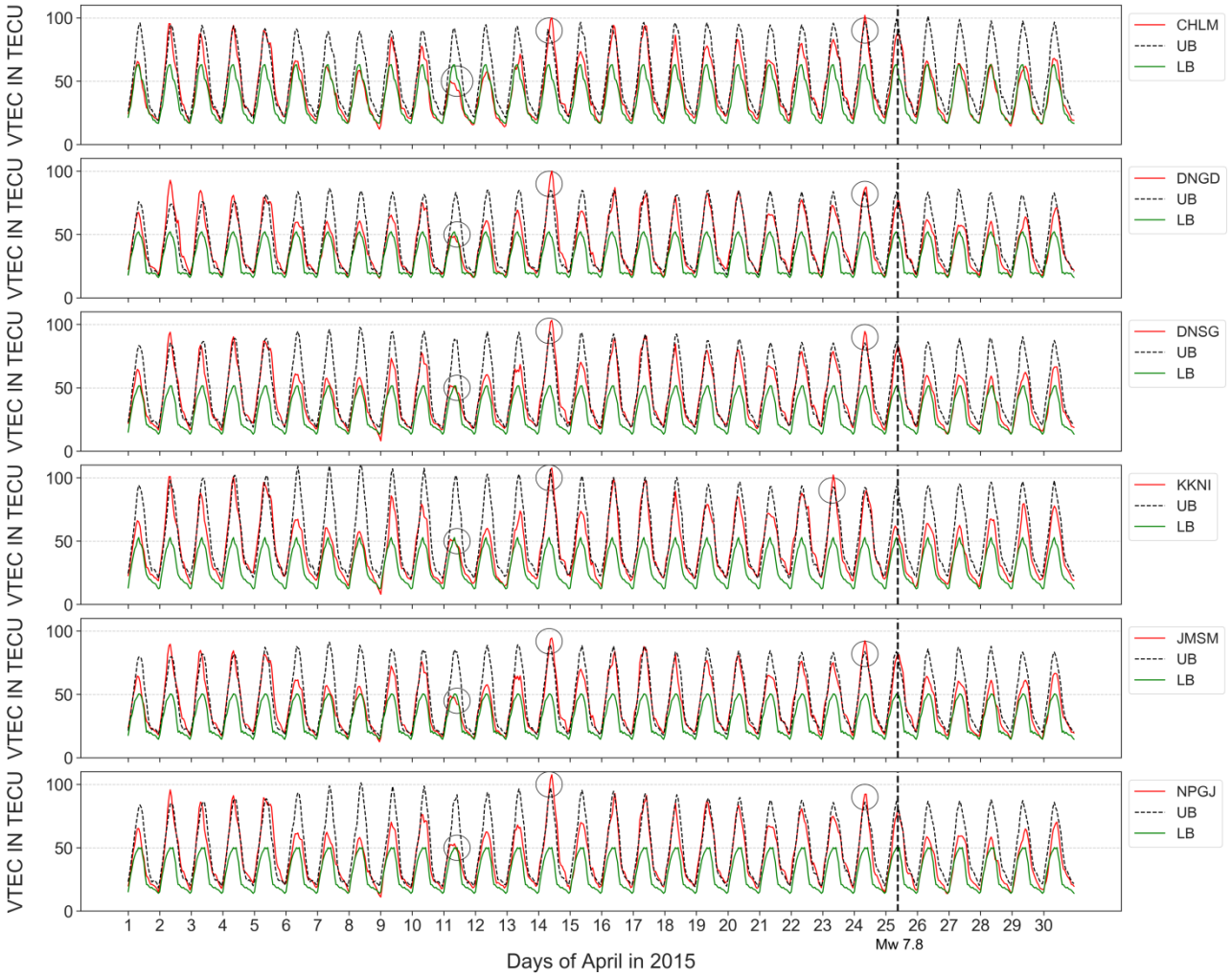

Fig.1. VTEC values observed in the TEC unit for the period of one month computed from CHLM, DNGD, DNSG, KKNI, JMSM and NPGJ represent the TEC variation for the month of April. The circles represent the anomalous TEC variation. Anomalies are marked when TEC crosses upper and lower bounds.

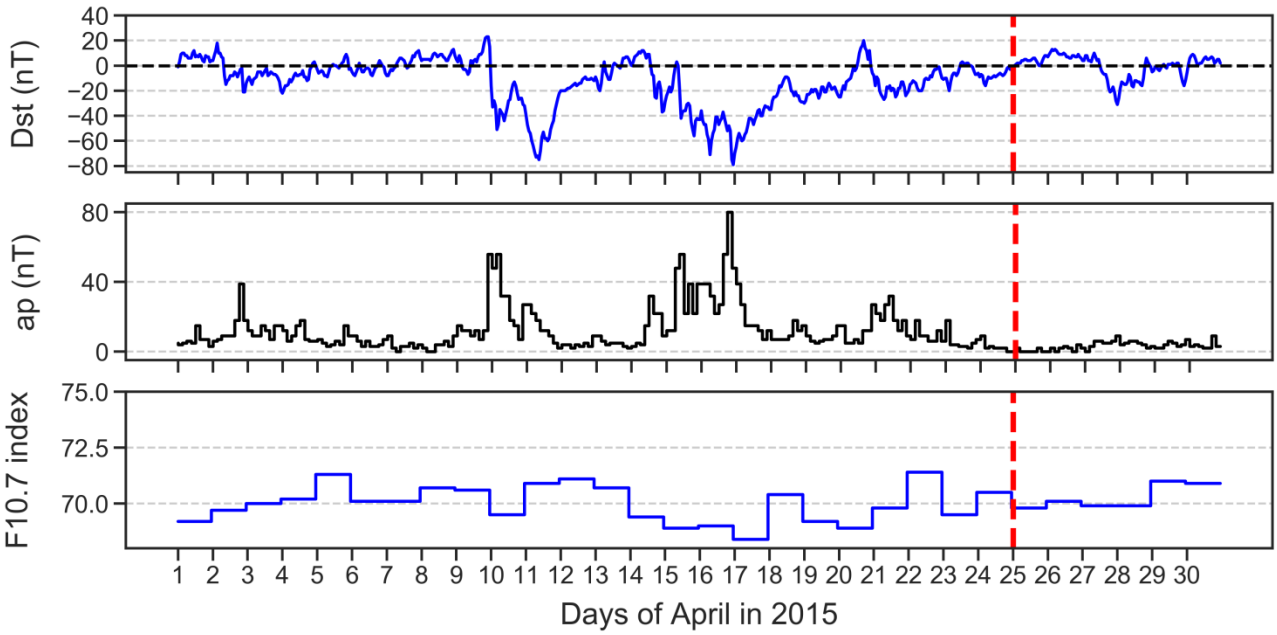

Fig.2. Variation in Dst-index, ap-index and F10.7 index during the Nepal earthquake (25 April 2015)

Comparison of quiet day TEC with that of earthquake day (25th April 2015)

Fig 3 shows the variation of TEC level during the earthquake event of 25 April 2015 in comparison to the mean TEC of topmost five quietest days of the same month at DNGD, DNSG, JMSM, KKNI, NPGJ and CHLM stations. The trend of diurnal variation of average VTEC seems to be followed at all the stations, minimum in a pre-dawn, a continuous inclination in the early morning followed by an afternoon with maximum TEC value and then gradually decreases after the sunset. The value of VTEC during "earthquake day" is exceeding the "quiet day" from some time before the earthquake event. Significant increment on VTEC can be seen during the earthquake period. The VTEC reached to the maximum point at ~ 8:00 UT (13:45 LT). It is found to be recovered slowly but was greater than the quiet day value throughout the day. The increment in VTEC during earthquake events ranges from ~ 1.8 to 4.6 TECU at the different stations at various distances from the epicentre of the earthquake.

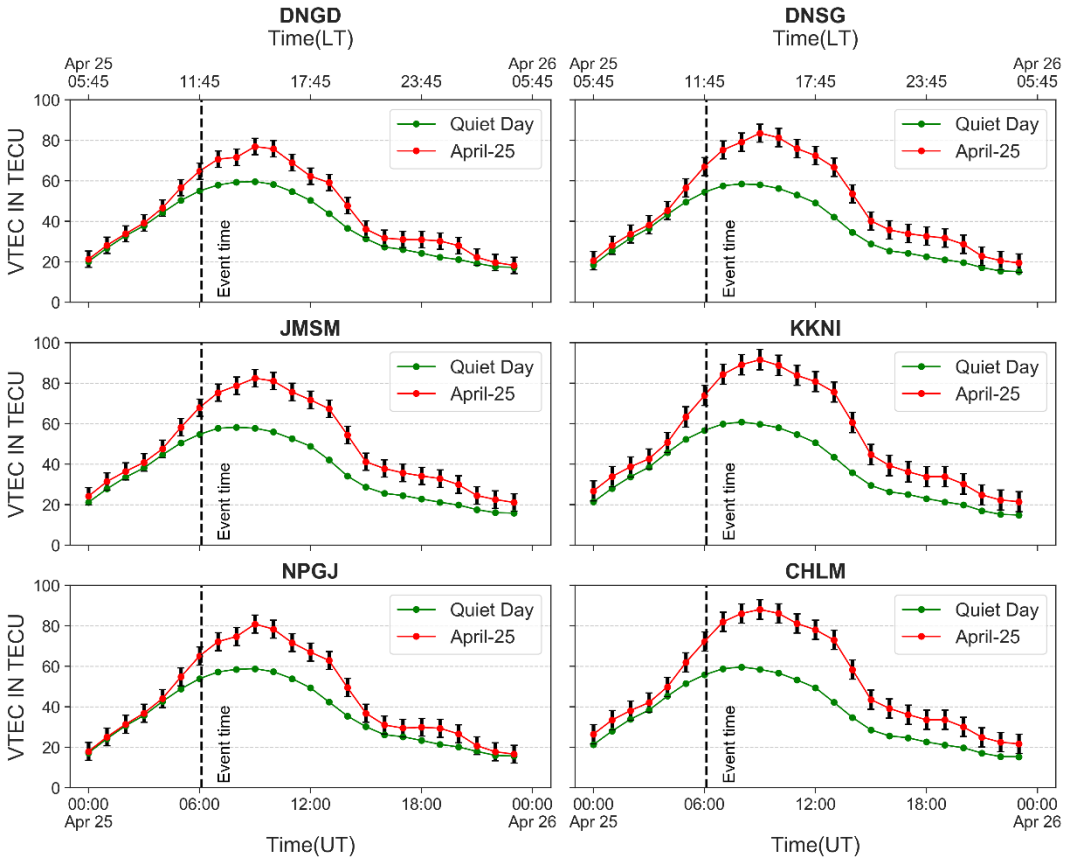

Fig.3. Comparison of TEC at six different stations during the earthquake of 25 April 2015 with the mean TEC of most five quietest days of the month. The vertical bar at earthquake day represents the standard error.

Deviation in VTEC on earthquake day from a quiet day

Fig 4 depicts that there was a significant increase in VTEC value during the earthquake event day compared to the quiet day. In this section, we study the deviation of GPS derived mean hourly VTEC in terms of percentage during the earthquake event day i.e. 25 April 2015 from mean of top 5 quietest days of the same month. The data of the top five quietest days were provided by the World Data Centre for Geomagnetism, Kyoto (http://wdc.kugi.kyoto-u.ac.jp/qddays/). Fig 4 describes that there was a high deviation in TEC right after the mainshock of earthquake event which was felt at 6:11 UT (~11:56 LT) and the almost constant increment remained for about 7 hours after the mainshock i.e. up to 14:00 UT. As observed from DNGD GPS station, the maximum VTEC difference between the day of the earthquake and the quiet day reached to 17 TECU whereas 25 TECU from DNSG and JMSM stations, around 32 TECU while observed from KKNI, 30 TECU from CHLM and 22 TECU from NPGJ GPS stations. The high deviation of VTEC on event day from the quiet day was observed during the time interval of 6:00 UT to 14:00 UT. However, there was a relatively small deviation of less than 10% before the mainshock and after 7 hours of mainshock i.e.

after 14:00 UT in all stations as witnessed from Fig 4. It is noteworthy that, throughout the earthquake event day the positive deviation of VTEC was recorded.

It was also noticed that the deviation decreased, with an increase in distance of the station from the epicentre. The DNGD station which is ~409 km from the epicentre showed the maximum deviation of only 17 TECU whereas deviation up to 32 TECU was spotted from KKNI GPS station which is only 71.9 km away from the epicentre. TEC variation is found to increase as the epicentre distance decreases which was also supported in earlier studies (Sharma et. al., 2017). The deviation of VTEC from quiet days fairly relates with distance (see table 1) of the station from the epicentre of the earthquake. Since earthquake event day was also the geomagnetically quiet day so, increment in VTEC during and after the earthquake event compared to other quiet days disclosed that there was momentous relation between seismic activity like earthquake and the ionospheric TEC.

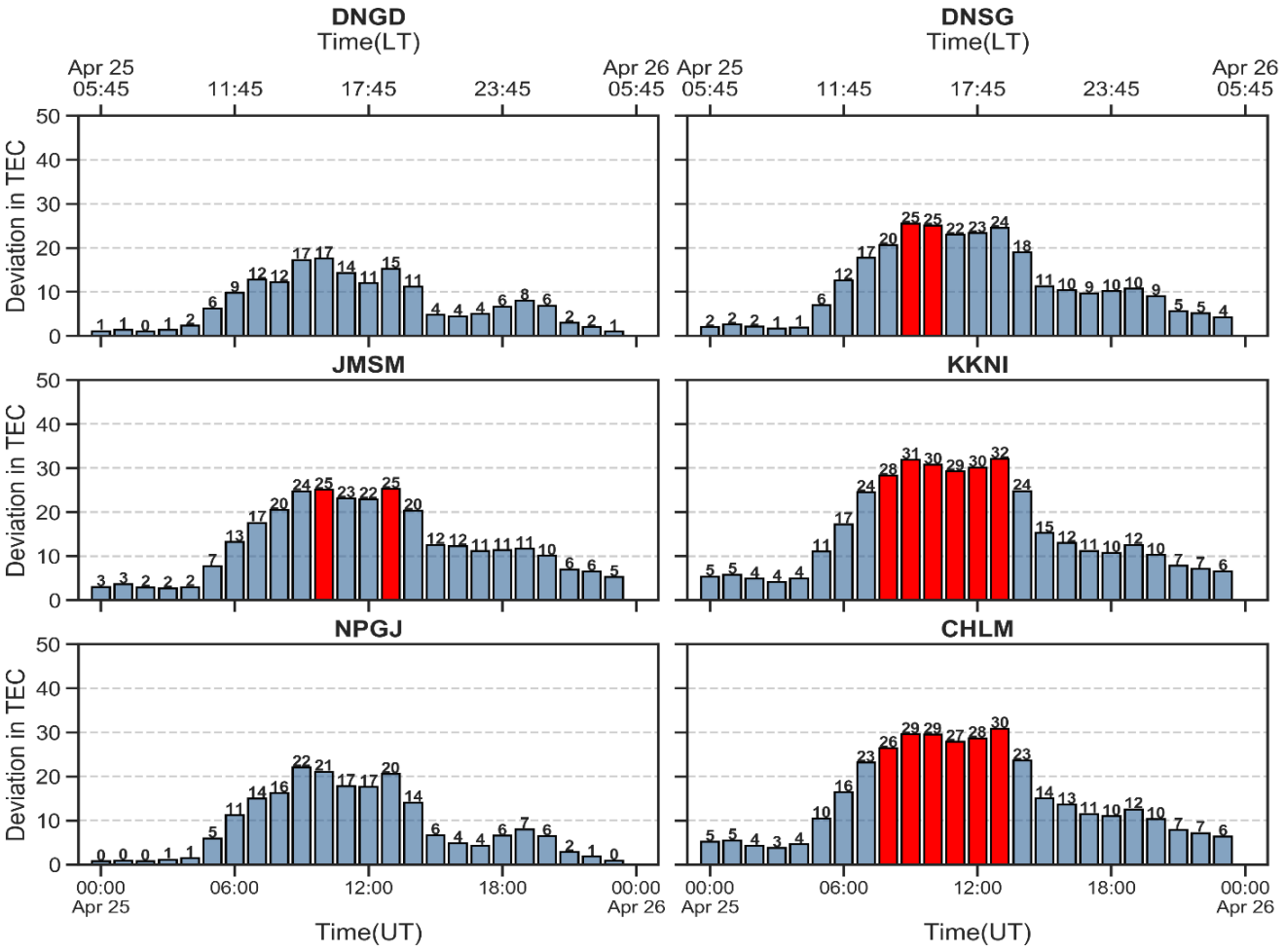

Fig.4. Deviation of TEC at six GPS stations on 25th April 2015 Nepal earthquake from the mean TEC of five quietest days of the month. The red bars represent a high deviation in TEC values.

Cross-Correlation Analysis

Fig 5(a) shows the plot of cross-correlation of mean hourly VTEC data of DNGD GPS station with mean hourly VTEC data of DNSG, JMSM, KKNI, CHLM and NPGJ GPS stations during the 2015 Gorkha earthquake. The horizontal axis ranges from -25 to 25 represents the time scale in hours and the vertical axis represents the cross-correlation coefficient. Time scales help to understand the lead or lag between the indices after establishing their correlation (Adhikari et al., 2018). The Fig displays the overlapping of all curves throughout the time lag of -24 to +24 with cross-correlation coefficient +1 at a zero-time lag. This reveals that there was a very strong positive association of mean hourly VTEC data of DNGD GPS station with other mentioned stations of Nepal during the earthquake event day i.e. 25 April 2015. This verified the similar pattern of diurnal variation of VTEC over Nepal (earthquake-affected region) during the earthquake event day.

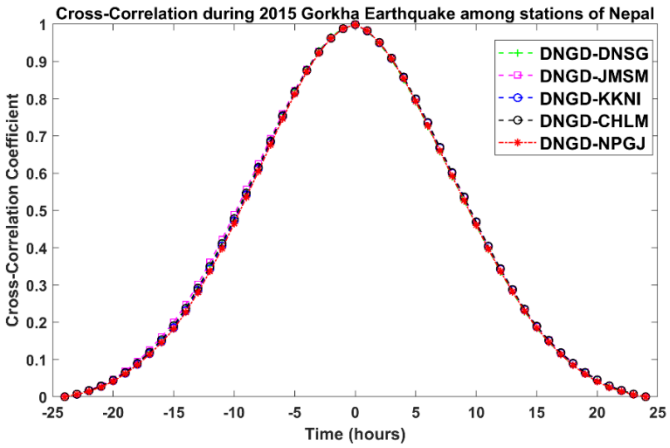

Fig. 5(a): Cross-correlation of VTEC derived from DNGD GPS station with DNSG, JMSM, KKNI, CHLM and NPGJ GPS station during the 2015 Gorkha event day.

In order to correlate the hourly mean VTEC of different GPS stations during the quiet day, we had added SGOC GPS station of Srilanka, IISC and HYDE GPS stations of south India along with GPS stations of Nepal mentioned in the above section. All the stations are located on mid and lower latitude regions. SGOC, HYDE and IISC are the stations which were not affected by the Gorkha earthquake 2015. Fig 5(b) depicts the cross-correlation of hourly mean VTEC of top five quietest days of April 2015 derived from SGOC GPS station with hourly mean VTEC derived from other stations. It demonstrated the strong positive correlation between mean hourly VTEC derived from SGOC station and mean hourly VTEC derived from DNGD, DNSG, CHLM, NPGJ, KKNI, JMSM, HYDE and IISC with correlation coefficient value of +1 at zero time lag. This suggests that during

the quiet day the similar variation of ionospheric VTEC can be observed on mid and lower latitude regions irrespective of their geographical locations.

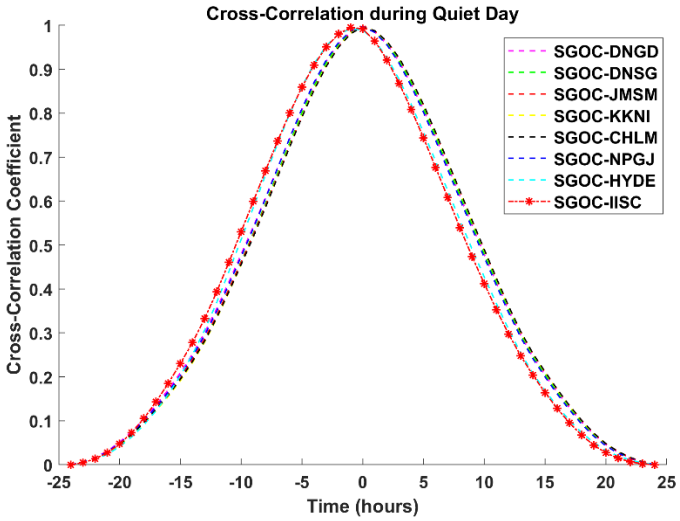

Fig. 5(b): Cross-correlation of VTEC derived from SGOC GPS station with DNSG, JMSM, KKNI, CHLM, NPGJ, HYDE and IISC GPS station during the quiet day of April 2015.

Fig 5(c) shows the cross-correlation of SGOC GPS station with other stations during the earthquake event day of Gorkha earthquake 2015. In the Fig, the magenta, yellow, green, blue, black and cyan curves representing the cross-correlation of mean hourly VTEC derived from SGOC with DNGD, NPGJ, DNSG, KKNI, CHLM and JMSM GPS stations respectively are overlapped throughout the time interval of -24 to +24 with cross-correlation coefficient of 0.8 at a time lag of -5 hours. This suggests that VTEC derived from DNGD, NPGJ, DNSG, KKNI, CHLM and JMSM stations i.e. earthquake-affected stations lead SGOC by 5 hours before they get correlated. But the red stared (SGOC-IISC) and blue squared (SGOC-HYDE) line has reached the cross-correlation coefficient of +1 at zero time-lag. This means VTEC derived from SGOC and IISC as well as HYDE stations were strongly correlated during the earthquake event day. This result revealed that the VTEC from GPS stations which were not affected by earthquake shows less correlation with some lag in time with VTEC derived from earthquake-affected stations whereas it showed perfect correlation with VTEC from stations not affected by the earthquake. The results obtained from the cross-correlation analysis supports that the increase in TEC value reported in the above section was solely due to the Earthquake event.

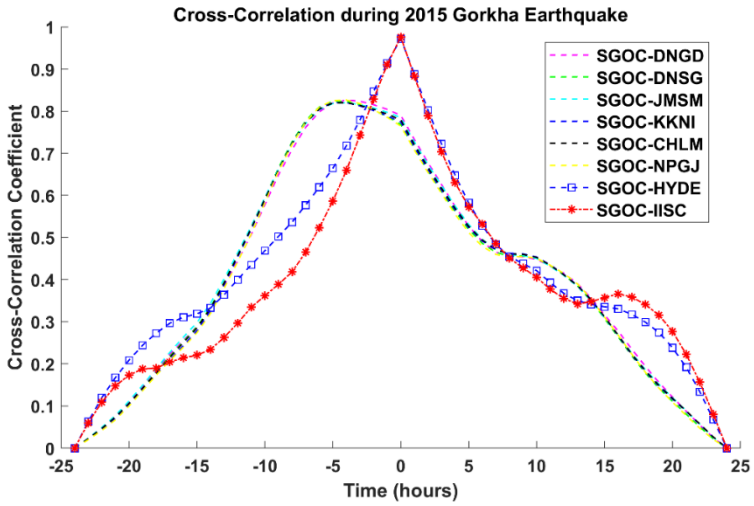

Fig. 5(c): Cross-correlation of VTEC derived from SGOC GPS station with DNSG, JMSM, KKNI, CHLM, NPGJ, HYDE and IISC GPS station during the earthquake event day of Gorkha earthquake 2015.

Since the cross-correlation is the standard method to estimate the degree to which two different series are correlated, this technique compares and evaluates the information between two time series of the included parameters as a function of a time lag (Finch & Lockwood, 2007; Mannucci et al., 2008). In addition, we found that the GPS TEC among the earthquake-affected stations was correlated with each other, as indicated by the cross-correlation technique. No noticeable lag has been found between the parameters discussed, which indicate a clear correlation between the specified stations. In these events, the GPS TEC response to the seismic activity is fairly rapid, as reflected by a zero-time lag value. All these stations that are affected by earthquake correspond to the similar change in global electric circuit produced by the gathering of ions in the atmosphere originating due to the development of stress in the crustal region prior to an earthquake (Pulinets, 2004; Friedemann and Kulahci, 2009). On the other hand, the decreased cross-correlation coefficient with a low time lag value between the stations which are not affected by earthquake accounts for the fewer perturbations on the ionospheric TEC during the event day. This indicates that the findings obtained are encouraging because, in future days, the space weather associated with the impact of the earthquake can easily be predicted by precise measurements of lead or lag in the response of the GPS TEC linked with seismic events.

Global Ionosphere Map

Figs 6, 7 and 8 define the contrast across the globe in TEC at a daily 2-hour UT interval on the day before, during and after the 2015 April 25 Earthquake. The contour along with the colour gradient represents the global TEC intensity. The high to low TEC activity ratio can be compared at any spatiotemporal location for the assessment of changes in the ionosphere that are evolved during the day. Figs reveal ionospheric maps based on geographical longitude and latitude over a global scale,

produced using various GPS stations in Nepal. Global contour plot indicates a transition in TEC with a gap of 2 hours beginning at 00:00 UT. The equatorial area comprises optimum spatial and temporal variations of the TEC and includes various characteristics of the ionosphere including the anomaly of the equatorial system and scintillation (Paulo de Oliveira, 2009). Thus, the emphasis is on the band of latitudes 26°-31°N, and longitudes 80°-89°E.

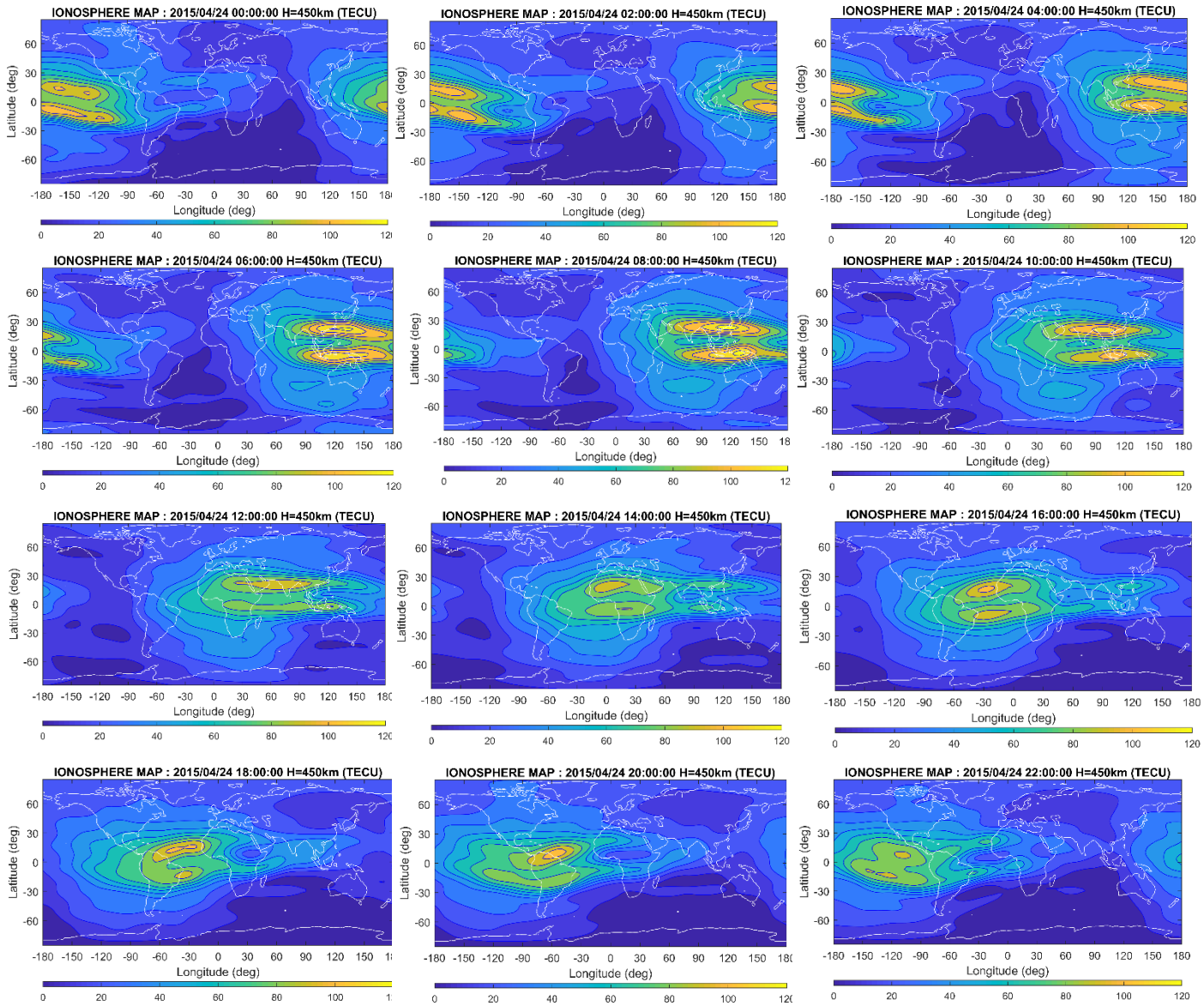

Fig.6. Global GPS-TEC maps on of 24th April 2015 at regular interval of 2 hours in UT.

At 00:00 UT-02:00 UT on 24 April, TEC content is high across the Pacific Ocean relative to other parts of the map. At 04:00 UT, the mild intensification of TEC as initially seen spreads to Indonesia, New Guinea and the Philippines and becomes intense at 06:00 UT. At this point, the Vietnam, Singapore and Southern China sectors are showing substantial TEC relative to the others. At 08:00 UT, there is a slight increase in TEC in the Eastern African region. From 08:00 UT-10:00 UT, the main concentration of TEC is located at lower latitude (-30 ° S to -30 ° N) between the regions of Indian and Southern China and is slowly moving towards Eastern Africa via the Arabian Sea. From

12:00 UT to 14:00 UT, TEC concentration is lower than the previous few hours and mild intensification of TEC is seen over Northern Africa. At 14:00 UT, TEC concentration is observed to be shifting towards South American region via Northern Atlantic Ocean from Africa. TEC is more pronounced towards the Atlantic at 16:00 UT and more pronounced over the western regions of Africa between 16:00 UT and 20:00 UT. There is a comparatively high TEC accumulation over the low latitude Atlantic regions (0 °-20 ° N) at 18:00 UT. From 20:00 UT-22:00 UT, South America's lower latitudinal regions exhibit extreme TEC. After 22:00 UT, TEC value decreases until the early hours of 25 April between -30° to 30° latitude across the Pacific Ocean, indicated by dark yellow colour. On 24 April, the most extreme TEC fluctuation is observed between 8 UT-10 UT over most of China and India's lower latitudinal area, while North American regions and Australian sectors display minimum TEC concentration throughout the day.

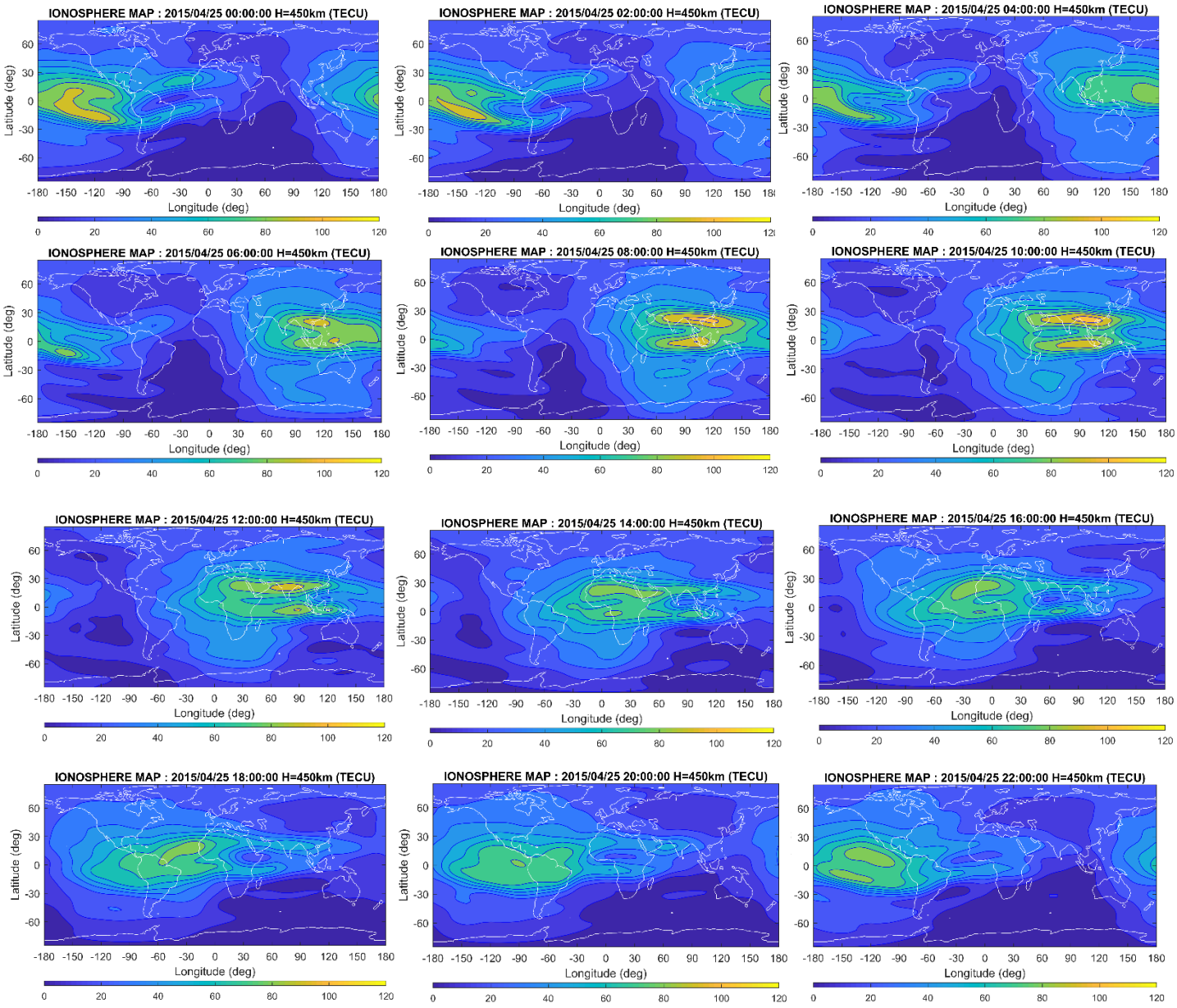

Fig.7. Global GPS-TEC maps on 25th April 2015 at regular interval of 2 hours in UT.

At 00:00 UT - 02:00 UT on 25th April, TEC content is supplementary over northern Pacific and Atlantic Ocean (40-60 TECU). At 04:00 UT, TEC concentration begins to intensify over the East China Sea, Indian region, Bay of Bengal, Indonesia and Malaysia and turns out to be extreme at 06:00 UT. At this point, compared to other parts of the globe, the Eastern China and Northern New Guinea regions display significant TECs. From 08:00 UT - 10:00 UT, TEC concentration rises significantly compared to the previous few hours in most of the Indian areas, Southern China, Nepal, Bhutan and the Indian Ocean (100-120 TECU) and by the end 10:00 UT the TEC concentration is observed to be shifting towards the Eastern and Central Africa. At 12:00 UT, lower latitudinal regions of Africa and India evinces mild TEC over the region. This intensification lasts until 18:00 UT over Western African regions and the North Atlantic Ocean, and until 14:00 UT over northern African regions. From 20:00 UT-22:00 UT, the North-West regions of South America had a moderate TEC over the area relative to the preceding hours. After 22:00 UT, TEC value decreases until the early hours of 26 April between -30° to 30° latitude across the Pacific Ocean indicated by dark yellow colour Between the period of 06:00 UT – 12:00 UT, TEC concentration is remarkably high near to the regions of Nepal ranging from 100-120 TECU, which continues until the end of the day through the equatorial plane covering low latitudinal regions.

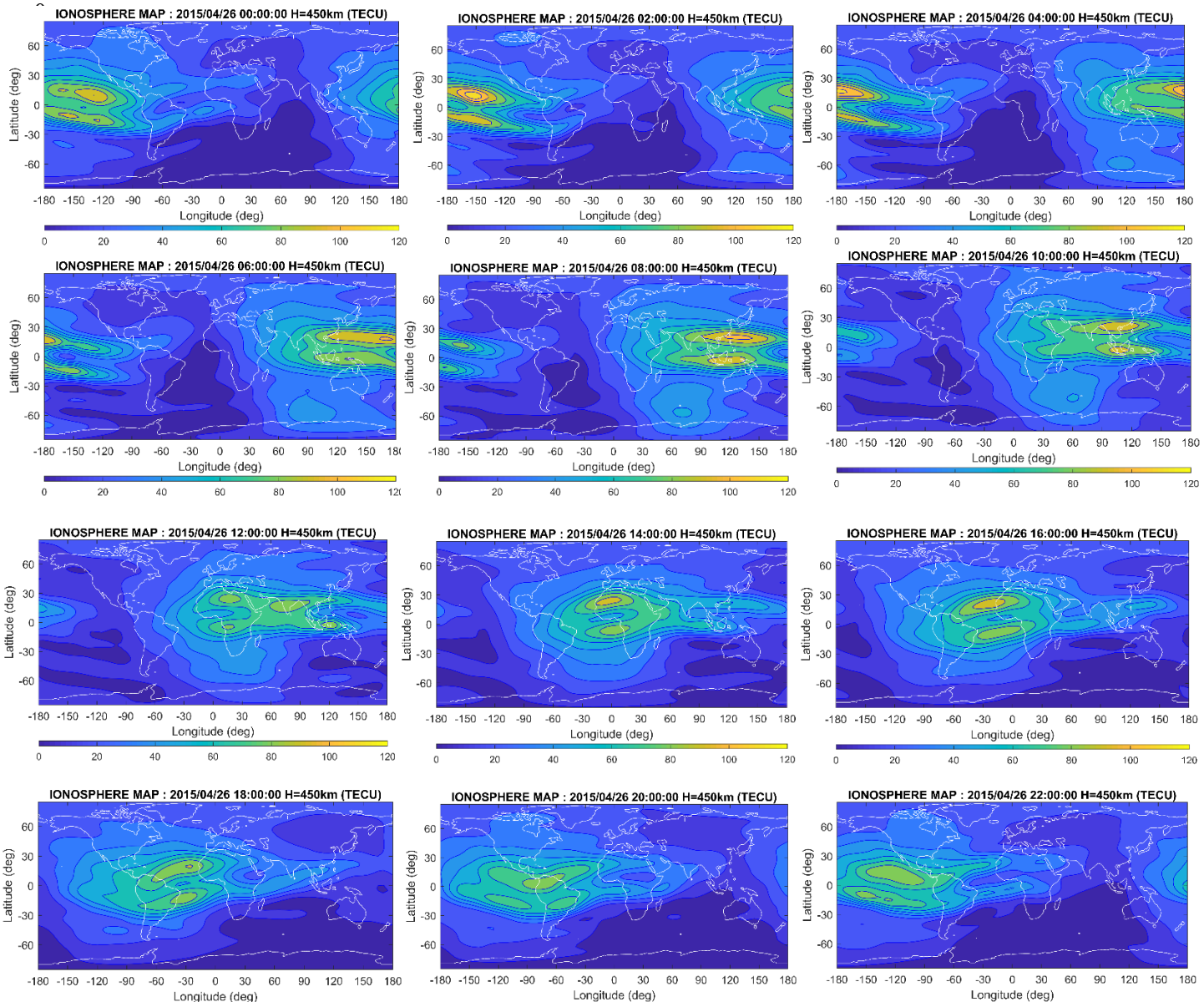

Fig.8. Global GPS-TEC maps on 26th April 2015 at regular interval of 2 hours in UT.

Following the earthquake day, the Equatorial and Low Latitude regions are observed in the Pacific Ocean with increased TECs while the Indian belts are showing minimum effects. Mild TEC variation is observed near Northern Australia, Guinea, Indonesia and East China at 06:00 UT. At 08:00 UT on 26 April, highly amplified TEC effects are seen across southern China and near Indonesia, including parts of Malaysia and the Indian regions, depicted by a dark yellow colour. Soon the TEC variations get prolonged over India, Nepal and China together with Eastern African zones at 10:00 UT near-equatorial planes. The TEC concentration is seen to be diminished over the Indian, Southern China, including most African, regions at 12:00 UT, following adverse impacts on African and Indian belts. From 14:00 UT-18:00 UT, the lower part of South America displays extreme TEC over the northern African regions (0-30 ° N), which stretch along the Atlantic Ocean. From 20:00 UT to the early morning hours of April 27, the TEC concentration decreased across the northern sector of South America along with the North Pacific Ocean. The most intense TEC is observed at 08:00 UT on 26 April, which remained between-30 ° to 30 ° latitude at 10:00 UT across the Indian and Southern China regions indicated by light yellow colour.

Conclusions

We have attempted to investigate TEC variations during Nepal earthquake of April 25, 2015, observed by GPS receivers, located in different parts of Nepal. The main conclusions of this work are drawn together and presented in this section.

1) The Nepal earthquake on 25th April 2015 with magnitude 7.8 was preceded by TEC anomalies as observed at a station closer to the epicentre (57 km) and three GPS stations at a distance of (1000-2570 km) from the epicentre. The most noticeable anomaly was observed on 14th and 24th April 2015 (one day before mainshock), although the earliest abnormality was observed on 11th April 2015 which was also observed in earlier studies (Sharma et al., 2017, 2018, 2019, 2020).

2) By analysing the data of geomagnetic indices for the same observation period, we observed that there was no geomagnetic storm i.e. geomagnetic quiet days before and after the mainshock of the earthquake. Thus, we can conclude that the TEC variations as observed were attributed due to seismogenic causes.

3) The analysis of deviation in VTEC on earthquake event day (also a geomagnetically quiet day) from the mean VTEC of top four quietest days showed that there was an abrupt rise in the value of GPS VTEC after the earthquake event relative to that of the geomagnetic quiet days and the high deviation persisted approximately 7 hours after the earthquake occurred.

4) The less deviation of VTEC observed on the GPS station which is far from epicentre compared to that of stations nearby suggests that there was a high increment in VTEC near to the epicentre and variation in ionospheric VTEC almost inversely depends upon the distance of GPS stations from the epicentre. As the intensity of earthquake decreases with distance from the epicentre, this spatial variation of VTEC can also be summarized as the outgrowth of ionospheric TEC perturbations with the intensity of the earthquake.

5) The cross-correlation between GPS derived VTEC on earthquake event day within stations of earthquake affected region (of Nepal) showed a strong correlation of VTEC with coefficient +1 at a zero-time lag. Similarly, cross-correlation study of VTEC on a quiet day among the stations of mid-latitude and lower latitudes (includes earthquake affected and unaffected stations) also showed a strong positive correlation with a peak at +1 at phase. On the other hand, during the earthquake event day, instead of taking same GPS stations for cross-correlation study, we only observed a strong positive association between VTEC derived from stations which were not affected by the earthquake (SGOC, IISC, HYDE) with a correlation coefficient of +1 at phase whereas all cross-correlation curves between VTEC derived from earthquake-affected and unaffected GPS stations displayed a peak at 0.8 with certain time-lag indicating less correlation between VTEC derived from earthquake-affected and unaffected regions. Overall cross-correlation findings have led to the conclusion that the increase in VTEC value in the earthquake event day relative to the quiet day is due to the seismic waves produced by the earthquake.

6) TEC Maps evince that most of the Indian regions, Southern China, Nepal regions were affected heavily explaining the onset effect of the earthquake. There were no significant fluctuations a day before and after the earthquake. All the Nepalese stations attain their highest TEC values during the event. TEC, when observed at Global Ionospheric Maps, prolongs towards lower or mid-latitudinal region (30 to -30 degree) through equatorial plane during the event.

As these naturally occurring phenomena overwhelm the Earth, we have observed abrupt modifications in ionospheric TEC data detected in different monitoring stations. By integrating

measurements based on the global impact of such natural events, we can monitor the response of TEC towards the seismic events and it could be used as a sophisticated tool to forecast the emergence of these natural events. Pulinets (1998) also concluded ionosphere-seismic consequences are an ongoing process and are a key cause of ionosphere variability and such consequences may be seen at least five days before an earthquake.

Acknowledgements

Co-author, Monika Karki's research work has been supported by University Grant Commission (UGC), Nepal as the MSc dissertation fellowship. Geomagnetic indices (ap and Dst) data are obtained from the OMNI (http://isgi.unistra.fr/geomagnetic_indices.php) site. Solar flux (F10.7) index data are downloaded from the OMNI (http://omniweb.gsfc.nasa.gov/form) site. Ground-based dual-frequency GPS TEC data are extracted from the UNAVCO Data Archive (https://www.unavco.org/data/gps-gnss/data-access-methods/dai2/app/dai2.html#) for the stations mentioned in Table 1. We would like to thank staff members of NASA and UNAVCO for making the data available.

References

Adhikari, B., Adhikari, R., Chapagain, N. P., Sapkota, N., Dahal, S., & Pandit, D. (2017). Daily, seasonal and monthly variation of middle-low latitudes magnetic field during low solar activity. *Discovery*, *53*(255), 181-190.

Adhikari, B., Dahal, S., Sapkota, N., Baruwal, P., Bhattarai, B., Khanal, K., & Chapagain, N. P. (2018). Field-Aligned Current and Polar Cap Potential and Geomagnetic Disturbances: A Review of Cross-Correlation Analysis. *Earth and Space Science*, *5*(9), 440-455.

Adhikari, B., Kaphle, B., Adhikari, N., Limbu, S., Sunar, A., Mishra, R. K., & Adhikari, S. (2019). Analysis of cosmic ray, solar wind energies, components of Earth's magnetic field, and ionospheric total electron content during solar superstorm of November 18–22, 2003. *SN Applied Sciences*, *1*(5), 453.

Adhikari, B., Dahal, S., Karki, M., Mishra, R. K., Dahal, R. K., Sasmal, S., & Klausner, V. (2020). Application of wavelet for seismic wave analysis in Kathmandu Valley after the 2015 Gorkha earthquake, Nepal. *Geoenvironmental Disasters*, *7*(1), 1-16.

Ciraolo, L., Azpilicueta, F., Brunini, C., Meza, A., & Radicella, S. M. (2007). Calibration errors on experimental slant total electron content (TEC) determined with GPS. *Journal of Geodesy*, *81*(2), 111-120.

Chen, P., Yao, Y., & Yao, W. (2017). On the coseismic ionospheric disturbances after the Nepal Mw7. 8 earthquakes on April 25, 2015 using GNSS observations. *Advances in Space Research*, *59*(1), 103-113.

598 Freund, F. T., Kulahci, I. G., Cyr, G., Ling, J., Winnick, M., Tregloan-Reed, J., & Freund, M. M.
599 (2009). Air ionization at rock surfaces and pre-earthquake signals. *Journal of Atmospheric and*
600 *Solar-Terrestrial Physics*, *71*(17-18), 1824-1834.

601 Haase, J.S., Dautermann, T., Taylor, M. J., Chapagain, N., Calais, E., Pautet, D., (2011).
602 Propagation of plasma bubbles observed in Brazil from GPS and airglow data. *Advances in Space*
603 *Research,* 47(10),1758-1776.

604 Kudela, K., Matisin, J., Shuiskaya, F. K., Akentieva, O. S., Romantsova, T. V., & Venkatesan, D.
605 (1992). Inner zone electron peaks observed by the "Active" satellite. *Journal of Geophysical*
606 *Research: Space Physics*, *97*(A6), 8681-8683.

607 Kotz, S., Johnson, H. L., Read, C. B., 1982, Encyclopedia of statistical sciences, 519.5, E5.

608 Liu, J. Y., Chen, Y. I., Pulinets, S. A., Tsai, Y. B., & Chuo, Y. J. (2000). Seismo-ionospheric
609 signatures prior to M≥ 6.0 Taiwan earthquakes. *Geophysical research letters*, *27*(19), 3113-3116.

610 Liu, J. Y., Chuo, Y. J., Shan, S. J., Tsai, Y. B., Chen, Y. I., Pulinets, S. A., & Yu, S. B. (2004). Pre-
611 earthquake ionospheric anomalies registered by continuous GPS TEC measurements. In *Annales*
612 *Geophysicae*, 22(5), 1585-1593.

613 Liu, J. Y., Chen, Y. I., Chen, C. H., Liu, C. Y., Chen, C. Y., Nishihashi, M., & Lin, C. H. (2009).
614 Seismoionospheric GPS total electron content anomalies observed before the 12 May 2008 Mw7. 9
615 Wenchuan earthquake. *Journal of Geophysical Research: Space Physics*, *114*(A4).

616 Liu, J. Y., Le, H., Chen, Y. I., Chen, C. H., Liu, L., Wan, W., ... & Chen, M. Q. (2011). Observations
617 and simulations of seismoionospheric GPS total electron content anomalies before the 12 January
618 2010 M7 Haiti earthquake. *Journal of Geophysical Research: Space Physics*, *116*(A4).

619 Oikonomou, C., Haralambous, H., & Muslim, B. (2016). Investigation of ionospheric TEC
620 precursors related to the M7. 8 Nepal and M8. 3 Chile earthquakes in 2015 based on spectral and
621 statistical analysis. *Natural Hazards*, *83*(1), 97-116.

622 Ohnaka, M. (2013). *The physics of rock failure and earthquakes*. Cambridge University Press.

623 Planinić, J., Radolić, V., & Vuković, B. (2004). Radon as an earthquake precursor. *Nuclear*
624 *Instruments and Methods in Physics Research Section A: Accelerators, Spectrometers, Detectors*
625 *and Associated Equipment*, *530*(3), 568-574.

626 Píša, D., Němec, F., Parrot, M. and Santolík, O., 2012. Attenuation of electromagnetic waves at the
627 frequency~ 1.7 kHz in the upper ionosphere observed by the DEMETER satellite in the vicinity of
628 earthquakes. *Annals of geophysics*, *55*(1).

629 Pulinets, S. A. (1998). Seismic activity as a source of the ionospheric variability. *Advances in Space*
630 *Research*, *22*(6), 903-906.

Pulinets, S. A., Boyarchuk, K. A., Hegai, V. V., & Karelin, A. V. (2002). Conception and model of seismo-ionosphere-magnetosphere coupling. *Seismo-Electromagnetics: Lithosphere-Atmosphere-Ionosphere Coupling*, 353-361.

Pulinets, S. A., Contreras, A. L., Bisiacchi-Giraldi, G., & Ciraolo, L. (2005). Total electron content variations in the ionosphere before the Colima, Mexico, earthquake of 21 January 2003. *Geofísica internacional*, *44*(4), 369-377.

Pulinets, S. A. (2007). Natural radioactivity, earthquakes, and the ionosphere. *Eos, Transactions American Geophysical Union*, *88*(20), 217-218.

Pulinets, S. A. (2009). Physical mechanism of the vertical electric field generation over active tectonic faults. *Advances in Space Research*, *44*(6), 767-773.

Sharma, G., Mohanty, S., & Kannaujiya, S. (2017). Ionospheric TEC modelling for earthquakes precursors from GNSS data. *Quaternary International*, *462*, 65-74.

Parashar, D., Sudeep, A., More, A., Patil, P., Walimbe, A., Mavale, M., & Amdekar, S. (2018). Total electron content and epicentral distance of 2015 Mw 7.8 Nepal earthquake revealed by continuous observations data. *current science*, *115*(1), 27.

Sharma, G., Ray, P. C., & Kannaujiya, S. (2019). Ionospheric Total Electron Content for Earthquake Precursor Detection. In *Remote Sensing of Northwest Himalayan Ecosystems* (pp. 57-66). Springer, Singapore.

Sharma, G., Saikia, P., Walia, D., Banerjee, P., & Raju, P. L. N. (2020). TEC anomalies assessment for earthquakes precursors in North-Eastern India and adjoining region using GPS data acquired during 2012–2018. *Quaternary International*.

Shi, K., Liu, X., Guo, J., Liu, L., You, X., & Wang, F. (2019). Pre-earthquake and coseismic ionosphere disturbances of the Mw 6.6 Lushan earthquake on 20 April 2013 monitored by CMONOC. *Atmosphere*, *10*(4), 216.

Shi, K., Guo, J., Liu, X., Liu, L., You, X., & Wang, F. (2020). Seismo-ionospheric anomalies associated with Mw 7.8 Nepal earthquake on 2015 April 25 from CMONOC GPS data. *Geosciences Journal*, 1-16.

Usoro, A. E. (2015). Some basic properties of cross-correlation functions of n-dimensional vector time series. *Journal of Statistical and Econometric Methods*, *4*(1), 63-71.

Wang, H. L., Chen, H. W., & Zhu, L. (2010). Constraints on average Taiwan Reference Moho Discontinuity Model—receiver function analysis using BATS data. *Geophysical Journal International*, *183*(1), 1-19.

663 Yao, Y., Chen, P., Wu, H., Zhang, S., & Peng, W. (2012). Analysis of ionospheric anomalies before
664 the 2011 M w 9.0 Japan earthquake. *Chinese science bulletin*, *57*(5), 570-510.
665 Finch, I., & Lockwood, M. (2007). Solar wind-magnetosphere coupling functions on timescales of
666 1 day to 1 year. https://doi.org/10.5194/angeo-25-495-2007
667 Mannucci, A. J., Tsurutani, B. T., Abdu, M. A., Gonzalez, W. D., Komjathy, A., Echer, E., ... &
668 Anderson, D. (2008). Superposed epoch analysis of the dayside ionospheric response to four intense
669 geomagnetic storms. *Journal of Geophysical Research: Space Physics*, *113*(A3).
670 Pulinets, S. A. (1998). Seismic activity as a source of the ionospheric variability. *Advances in Space*
671 *Research*, *22*(6), 903-906.
672 Klobuchar, J. A. (1991). Ionospheric Effects on GPS, Early Innovation columns, GPS World, 1991.
673 Available: http://gauss.gge.unb.ca/gpsworld/EarlyInnovationColumns/Innov.1991.04.pdf.
674
675

Table 1: Detailed information on GPS stations with their geographical latitude and longitude and distance from the epicentre.

GPS Station	**Geographical Latitude (^{0}N)**	**Geographical Longitude (^{0}E)**	**Distance from the epicentre (km)**
CHLM	28.2072	85.3141	57.1
NPGJ	28.1172	81.5953	307.61
KKNI	27.8007	85.2788	71.9
JMSM	28.8053	83.7433	115.8
DNGD	28.7544	80.5818	409.7
DNSG	28.3451	83.7635	95.6
HYDE	17.4173	78.5579	1358.64
SGOC	6.8921	79.8742	2427.802
IISC	13.0212	77.5704	1148.146

Figure1.

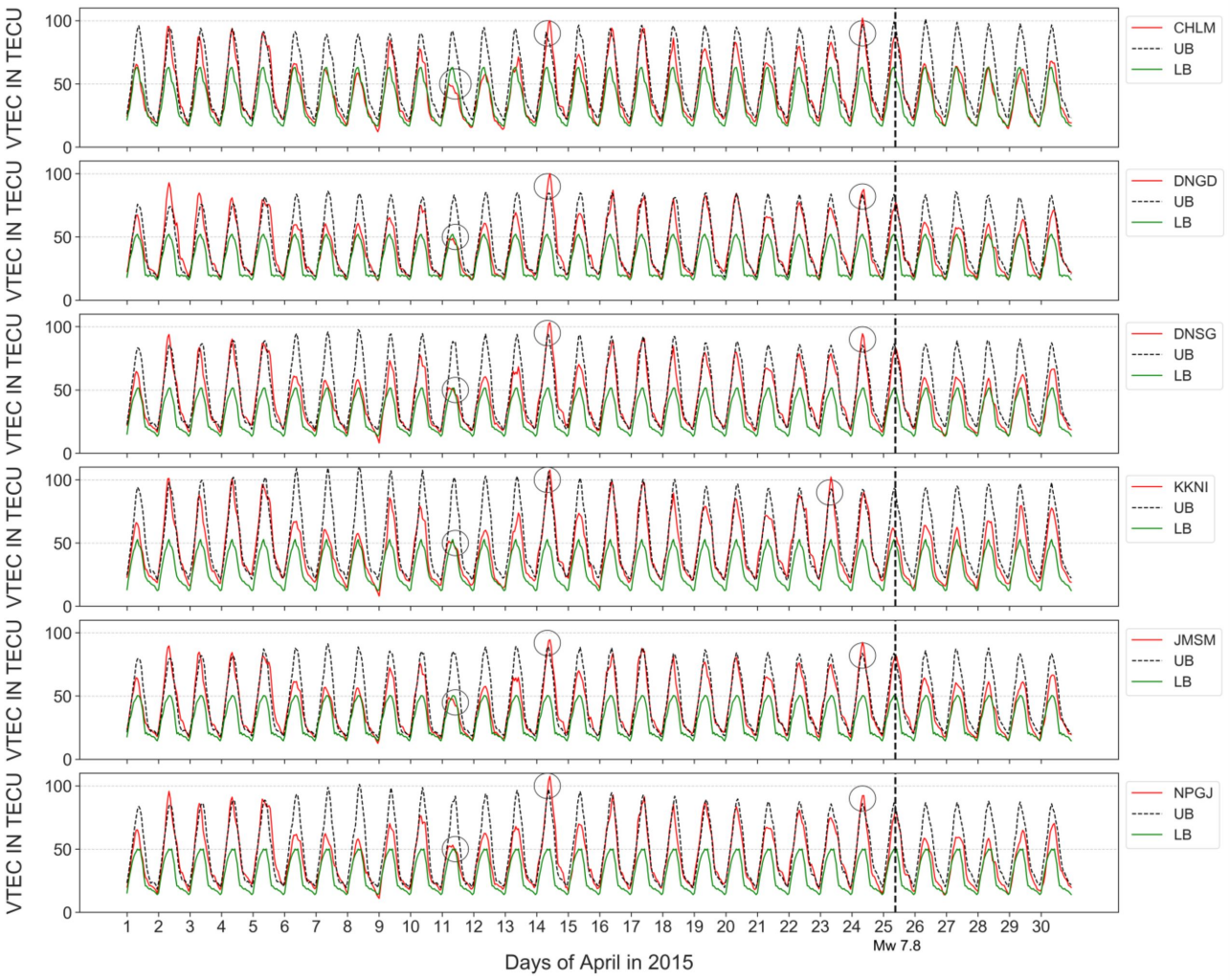
VTEC IN TECU
100
50
0
CHLM
UB
LB
DNGD
DNSG
KKNI
JMSM
NPGJ
1 2 3 4 5 6 7 8 9 10 11 12 13 14 15 16 17 18 19 20 21 22 23 24 25 26 27 28 29 30
Mw 7.8
Days of April in 2015

Figure2.

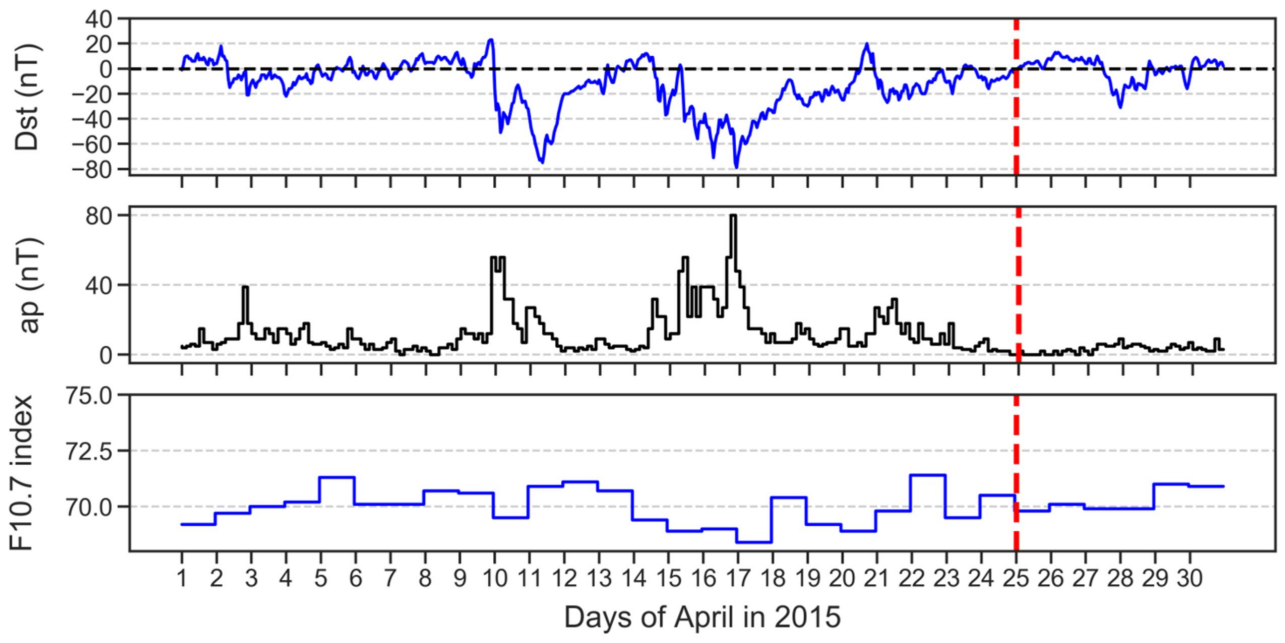
Dst (nT)
40
20
0
−20
−40
−60
−80
ap (nT)
80
40
0
F10.7 index
75.0
72.5
70.0
1 2 3 4 5 6 7 8 9 10 11 12 13 14 15 16 17 18 19 20 21 22 23 24 25 26 27 28 29 30
Days of April in 2015

Figure3.

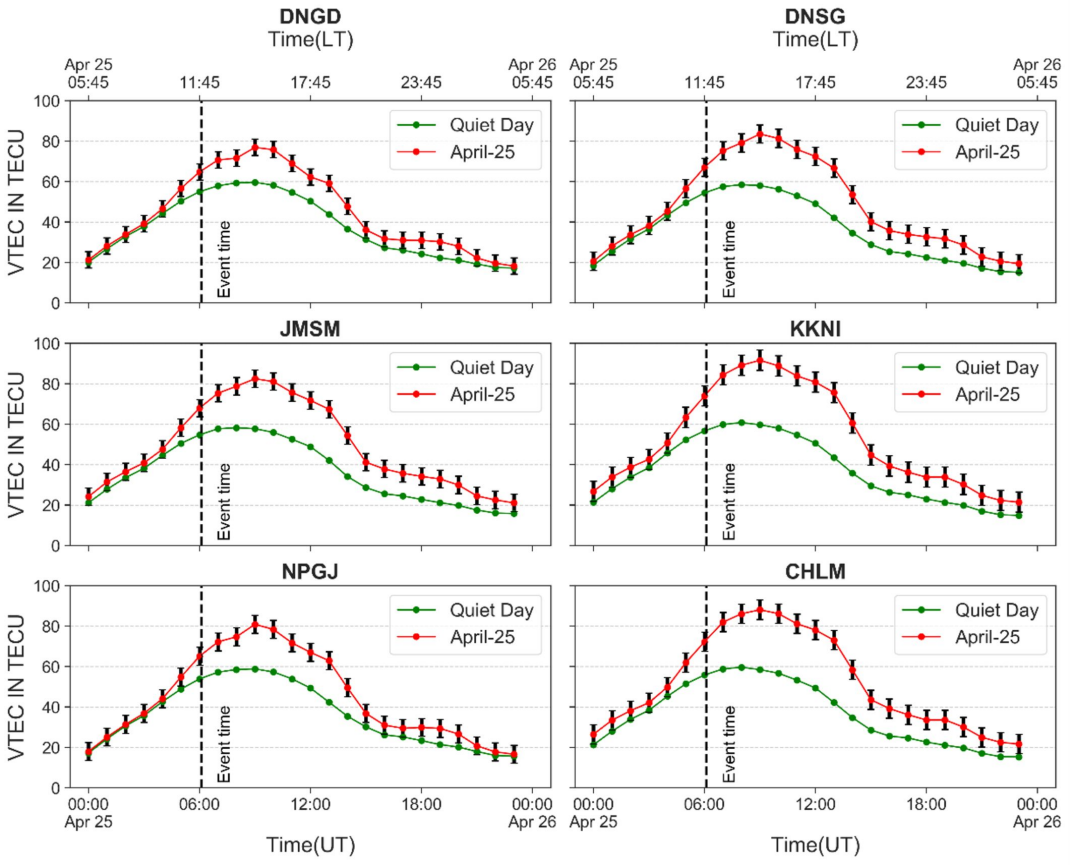
DNGD
Time(LT)
Apr 25
05:45
11:45
17:45
23:45
Apr 26
05:45
VTEC IN TECU
Quiet Day
April-25
Event time
DNSG
JMSM
KKNI
NPGJ
CHLM
00:00
Apr 25
06:00
12:00
18:00
00:00
Apr 26
Time(UT)

Figure4.

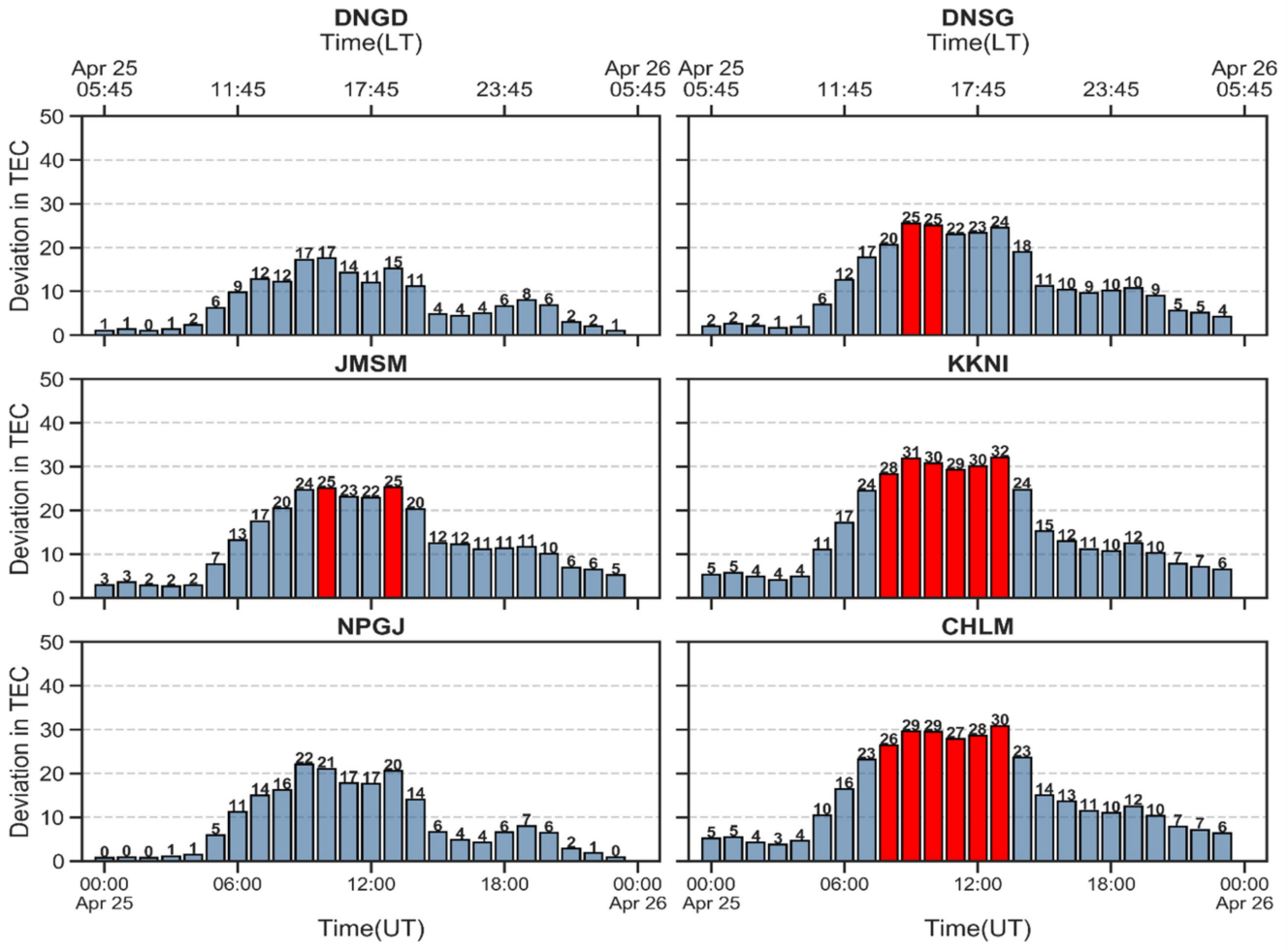
DNGD
Time(LT)
Apr 25
05:45
11:45
17:45
23:45
Apr 26
05:45
Deviation in TEC
DNSG
Time(LT)
JMSM
KKNI
NPGJ
CHLM
00:00
Apr 25
06:00
12:00
18:00
00:00
Apr 26
Time(UT)

Figure5(a).

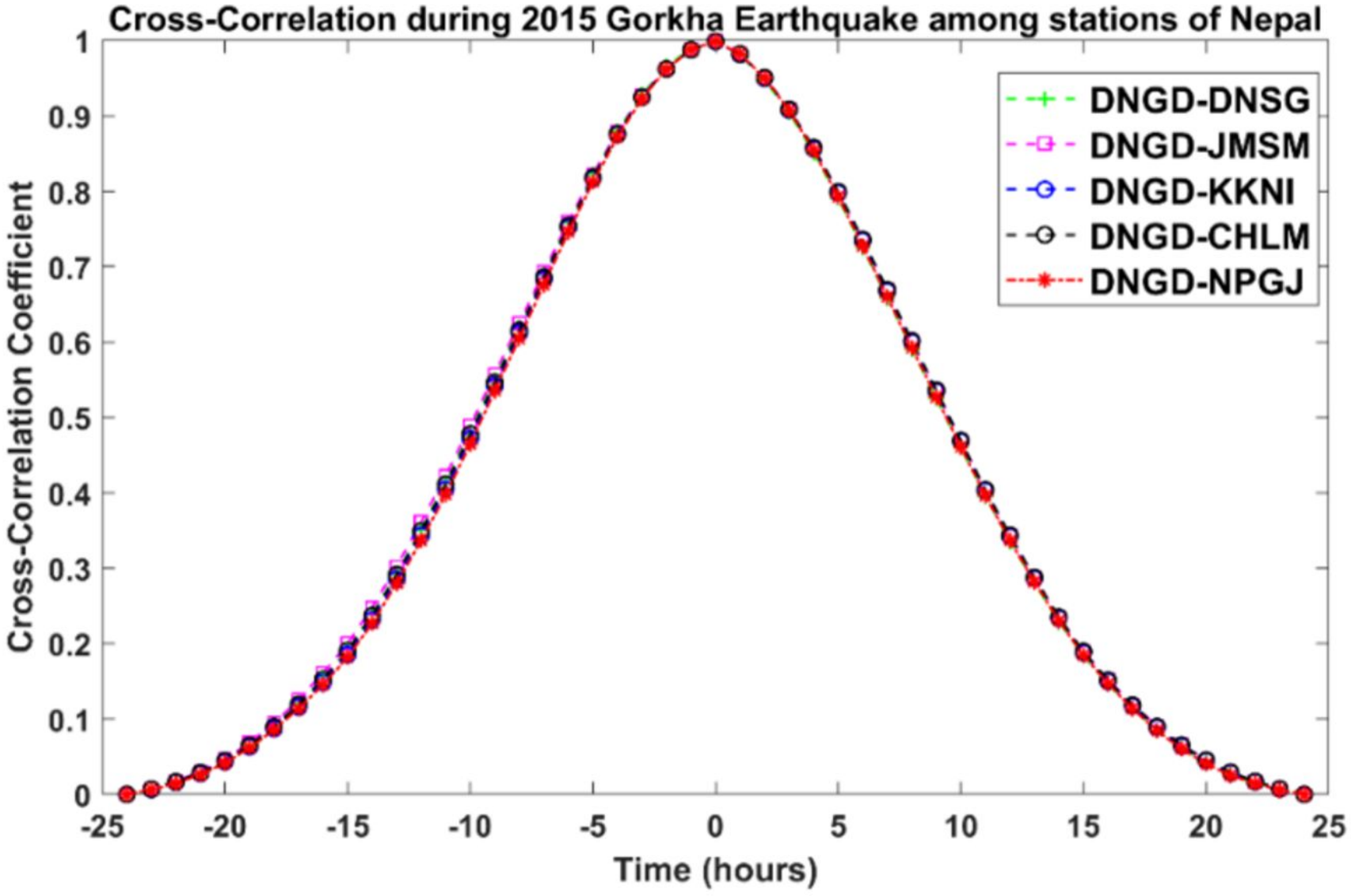
Cross-Correlation during 2015 Gorkha Earthquake among stations of Nepal
Cross-Correlation Coefficient
Time (hours)
DNGD-DNSG
DNGD-JMSM
DNGD-KKNI
DNGD-CHLM
DNGD-NPGJ
1
0.9
0.8
0.7
0.6
0.5
0.4
0.3
0.2
0.1
0
-25
-20
-15
-10
-5
0
5
10
15
20
25

Figure5(b).

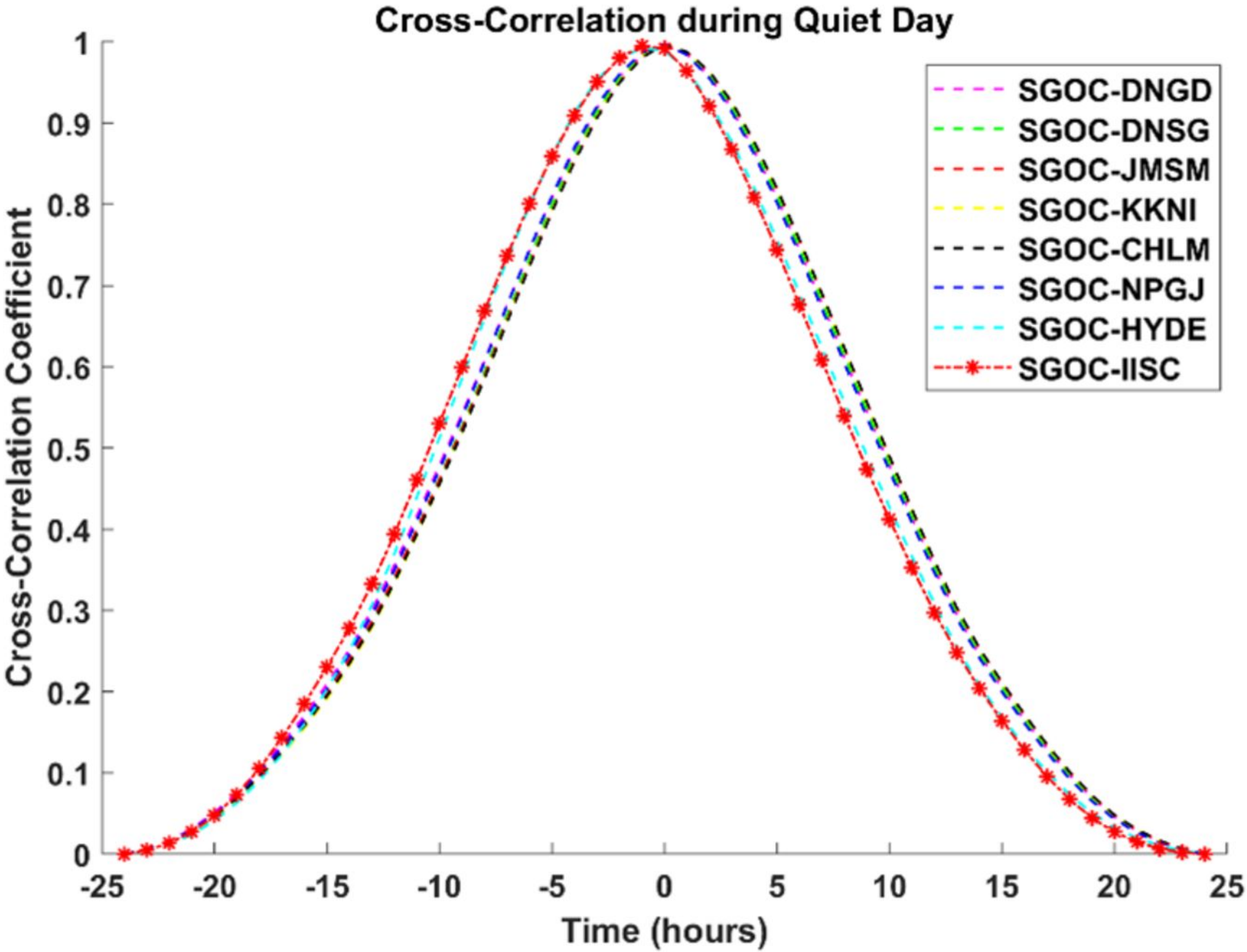
Cross-Correlation during Quiet Day
Cross-Correlation Coefficient
Time (hours)
SGOC-DNGD
SGOC-DNSG
SGOC-JMSM
SGOC-KKNI
SGOC-CHLM
SGOC-NPGJ
SGOC-HYDE
SGOC-IISC
1
0.9
0.8
0.7
0.6
0.5
0.4
0.3
0.2
0.1
0
-25
-20
-15
-10
-5
0
5
10
15
20
25

Figure5(c).

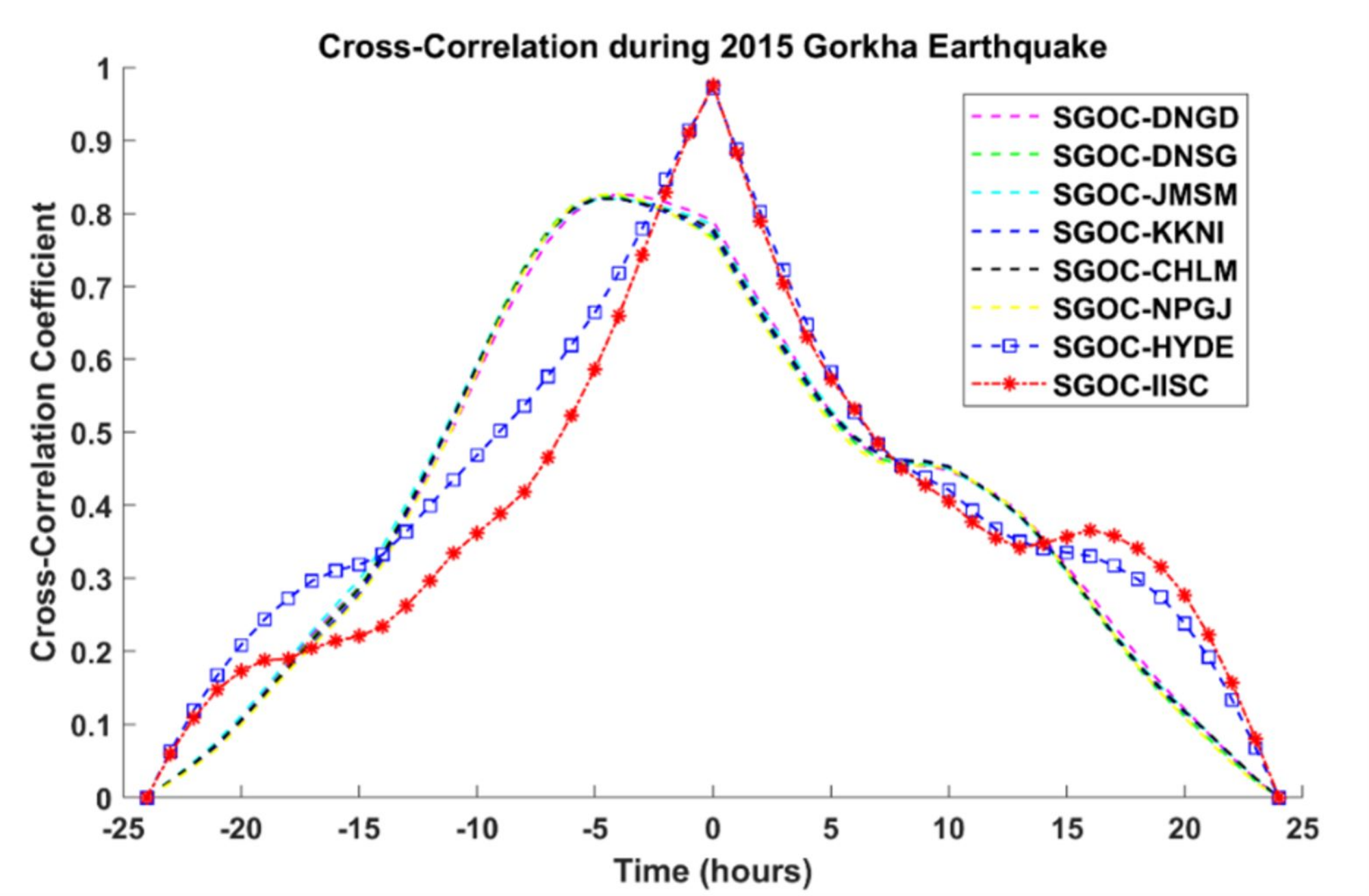
Cross-Correlation during 2015 Gorkha Earthquake
Cross-Correlation Coefficient
Time (hours)
SGOC-DNGD
SGOC-DNSG
SGOC-JMSM
SGOC-KKNI
SGOC-CHLM
SGOC-NPGJ
SGOC-HYDE
SGOC-IISC
0
0.1
0.2
0.3
0.4
0.5
0.6
0.7
0.8
0.9
1
-25
-20
-15
-10
-5
0
5
10
15
20
25

Figure6.

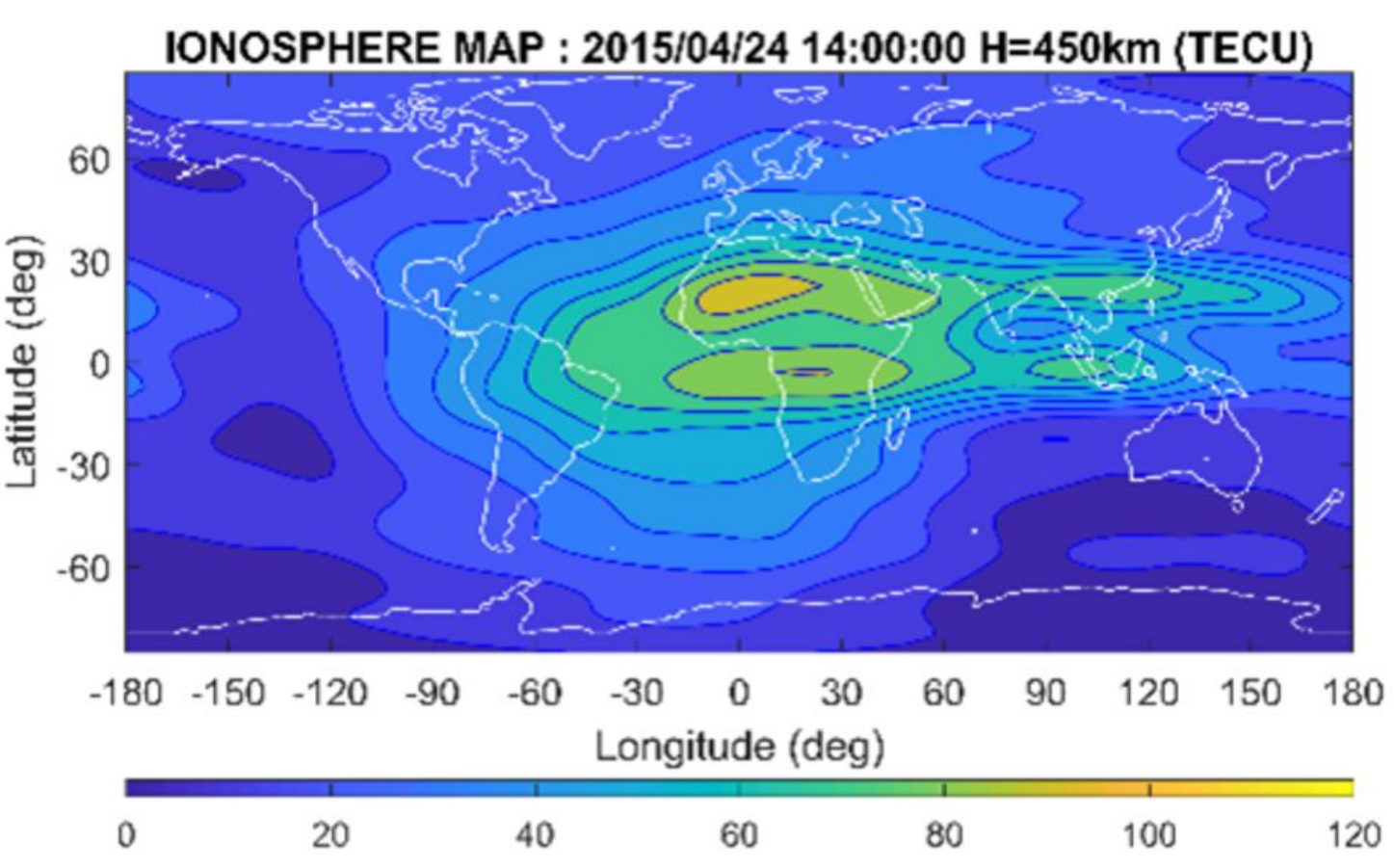
IONOSPHERE MAP : 2015/04/24 14:00:00 H=450km (TECU)
Latitude (deg)
60
30
0
-30
-60
-180 -150 -120 -90 -60 -30 0 30 60 90 120 150 180
Longitude (deg)
0 20 40 60 80 100 120

Figure7.

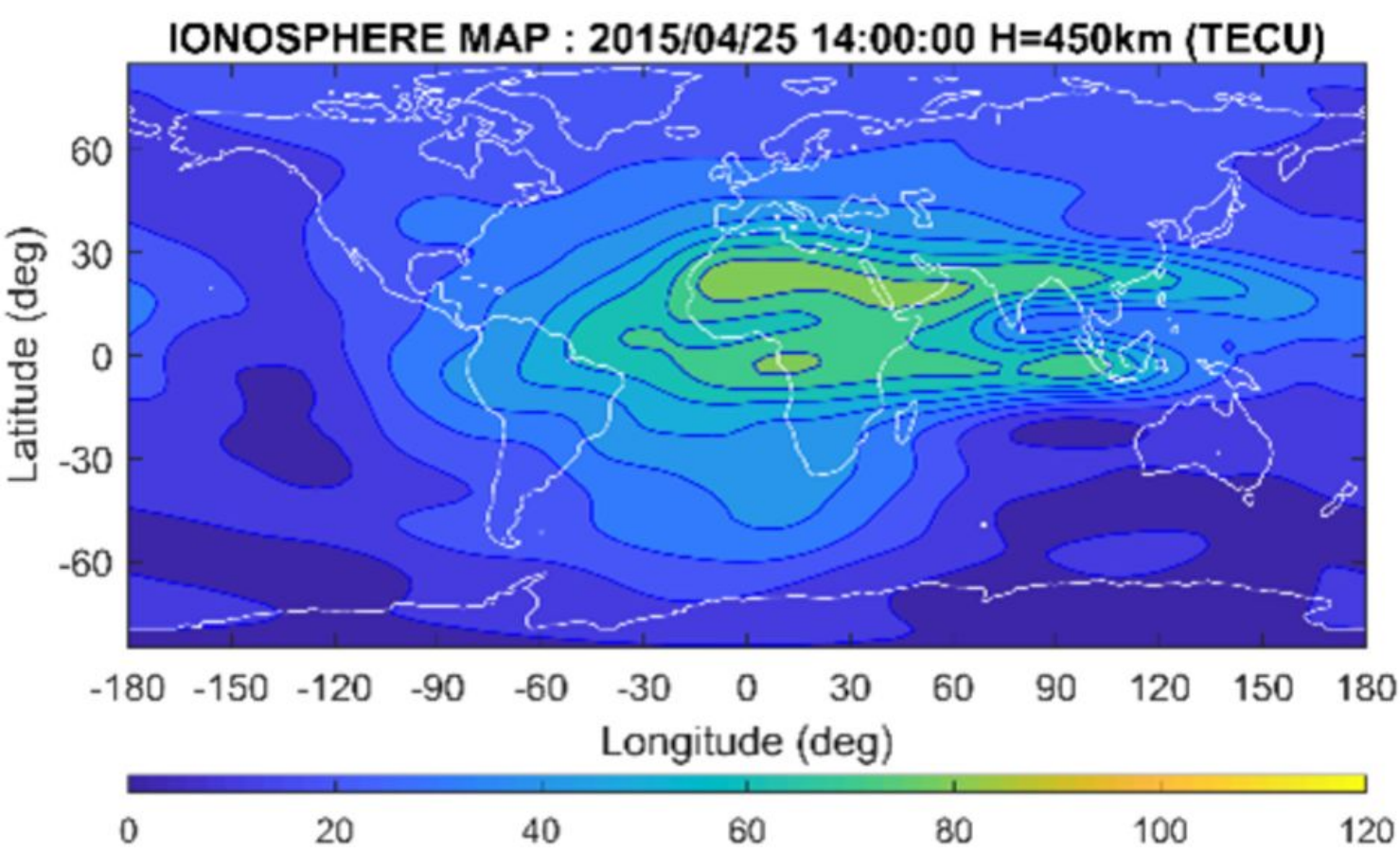
IONOSPHERE MAP : 2015/04/25 14:00:00 H=450km (TECU)
Latitude (deg)
60
30
0
-30
-60
-180 -150 -120 -90 -60 -30 0 30 60 90 120 150 180
Longitude (deg)
0 20 40 60 80 100 120

Figure8.

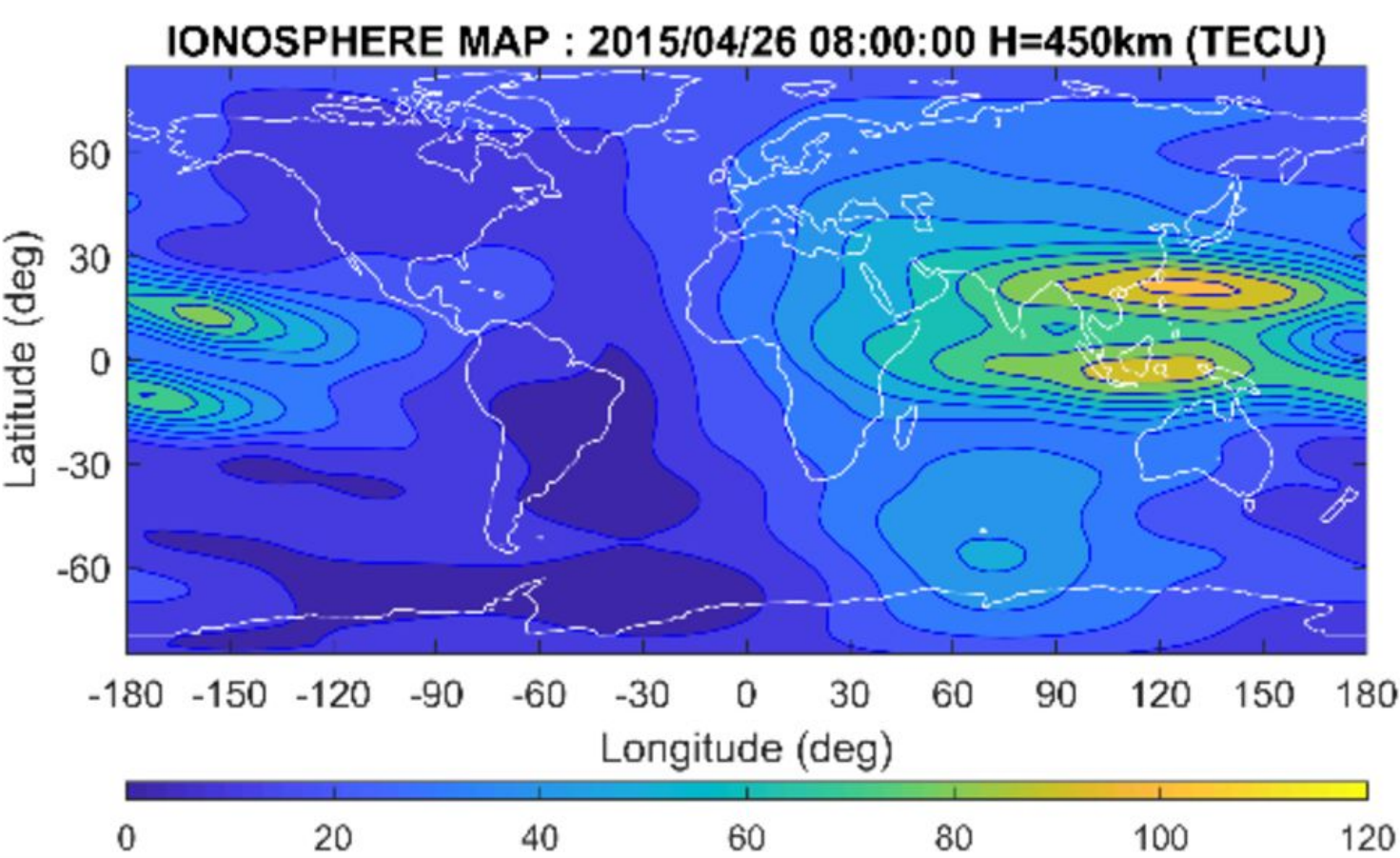
IONOSPHERE MAP : 2015/04/26 08:00:00 H=450km (TECU)
Latitude (deg)
60
30
0
-30
-60
-180 -150 -120 -90 -60 -30 0 30 60 90 120 150 180
Longitude (deg)
0 20 40 60 80 100 120